Cell Reports
Physical Science

CellPress
OPEN ACCESS

Report

Dynamic covalent macrocycles co-delivering genes and drugs against drug-resistant cancer

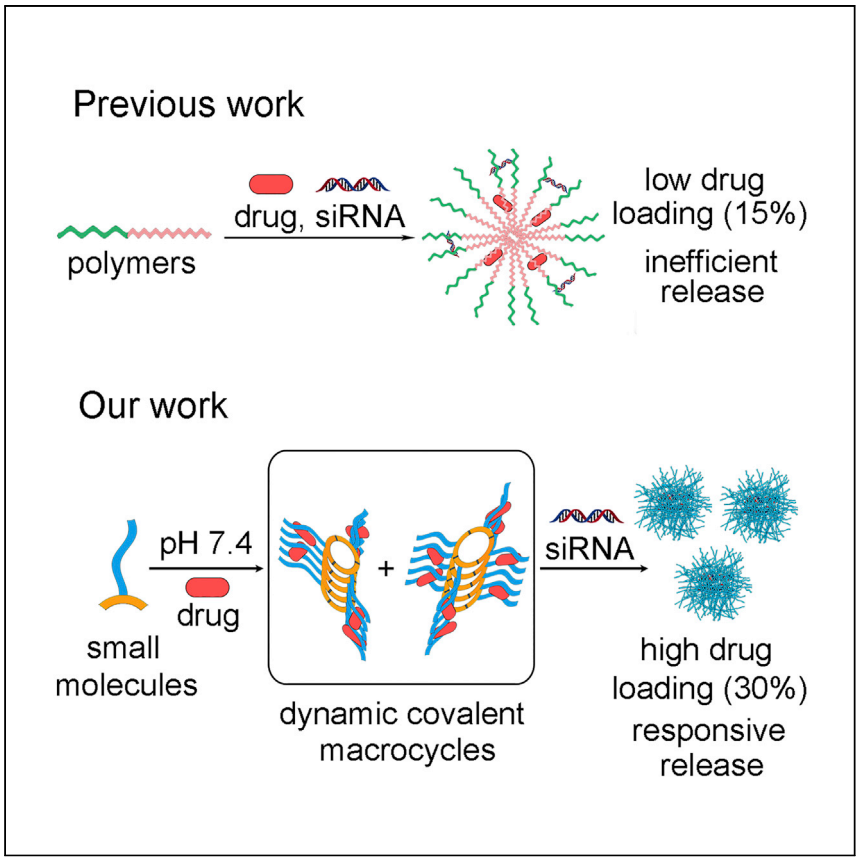

Yonglei et al. develop dynamic covalent macrocycles as new carriers through a reversible chemical reaction mediated by their non-covalent interaction with drugs. The thermodynamic control over the reaction equips the system with a strong drug-loading capacity, and by an additional loading of a gene, the resulting co-delivery system fights drug-resistant cancer efficiently *in vitro*.

Yonglei Lyu, Xiaoxia Wu, Anastassios C. Papageorgiou, Jinghui Yang, Xin Wang, Dawei Qi, Jianwei Li

jianwei.li@utu.fi

Highlights

Dynamic covalent macrocycles are promising carrier molecules for drug and gene delivery

Integrating synthesis and loading in one step is a smart way to co-delivery systems

Thermodynamic control over the synthesis enhances the loading capacity

Lyu et al., Cell Reports Physical Science *3*, 101150
November 16, 2022
https://doi.org/10.1016/j.xcrp.2022.101150

Please cite this article in press as: Lyu et al., Dynamic covalent macrocycles co-delivering genes and drugs against drug-resistant cancer, Cell Reports Physical Science (2022), https://doi.org/10.1016/j.xcrp.2022.101150

Cell Reports
Physical Science

CellPress
OPEN ACCESS

Report

Dynamic covalent macrocycles co-delivering genes and drugs against drug-resistant cancer

Yonglei Lyu,[1,2] Xiaoxia Wu,[1] Anastassios C. Papageorgiou,[3] Jinghui Yang,[1,2] Xin Wang,[1,2] Dawei Qi,[1] and Jianwei Li[1,4,5,6,7,8,*]

SUMMARY

Polymeric carriers have dominated the development of delivering chemotherapeutic drugs and genes against drug-resistant cancer. However, the biocompatibility, loading, and release capabilities of polymers are unsatisfactory. Here, we have advanced the delivery system by developing dynamic covalent macrocycles using a dithiol monomer through a thiol/disulfide exchange reaction to co-deliver doxorubicin (DOX) and small interfering RNA (siRNA). Our thermodynamically based macrocycles achieve a drug-loading content of 30.2%, whereas a disulfide polymer prepared from the same monomer under kinetic control cannot load DOX. In combination with siRNA, the macrocycles exhibit excellent delivery efficiency and enhanced anti-tumor efficacy *in vitro* without systemic toxicity. Our findings suggest that dynamic covalent chemistry offers a powerful strategy for exploring macrocyclic carriers that could replace conventional polymers for co-delivery systems, paving the way to more efficient clinic therapies.

INTRODUCTION

Combination therapy using effective drug molecules and functional genes such as small interfering RNA (siRNA) has been suggested as a powerful strategy against multiple-drug resistance (MDR).[1–6] Accordingly, co-delivery systems using various carriers have been developed.[7–10] Apart from inorganic particles, polymers are the main carrier molecules for co-delivery as they are stable and have chemical structures that are easy to modify.[11–13] However, polymeric co-delivery systems have inherent disadvantages. First, it is not easy to remove all the organic solvents that are trapped in the complex spatial structure of polymers during the synthesis or chemical modification process, which can lead to potential toxicity and safety problems for patients. Moreover, the stability of polymeric nanocarriers could cause inefficient drug and gene release rates in cancer cells, lowering their therapeutic efficacy.[14–16] Finally, the loading capacity of polymeric co-delivery systems is typically low.[17–19] Thus, it is highly desirable to explore biocompatible and stable, but responsive, co-delivery systems with a strong loading capacity.

Nanocarriers self-assembled by macrocycles should be a top candidate with the above-mentioned advantages for the co-delivery of genes and drugs.[20–22] Supramolecular macrocycles are usually featured with repeating units in their cyclic structures. The number of the repeating units of macrocycles is far fewer than that of polymers. This structural uniqueness endows them with multiple binding sites that can enhance their affinity with siRNA and loading capacity.[23–25] In addition, the relatively simplified structure of macrocycles eases their chemical modification, allowing them

[1]MediCity Research Laboratory, University of Turku, 20520 Turku, Finland

[2]Department of Chemistry, University of Turku, 20500 Turku, Finland

[3]Turku Bioscience Centre, University of Turku, Åbo Akademi University, 20520 Turku, Finland

[4]Hainan Provincial Key Laboratory of Fine Chem, School of Chemical Engineering and Technology, Hainan University, Haikou 570228, P.R. China

[5]Twitter: @uniturku

[6]Twitter: @medicityl

[7]Twitter: @jianwei_chem

[8]Lead contact

*Correspondence: jianwei.li@utu.fi

https://doi.org/10.1016/j.xcrp.2022.101150

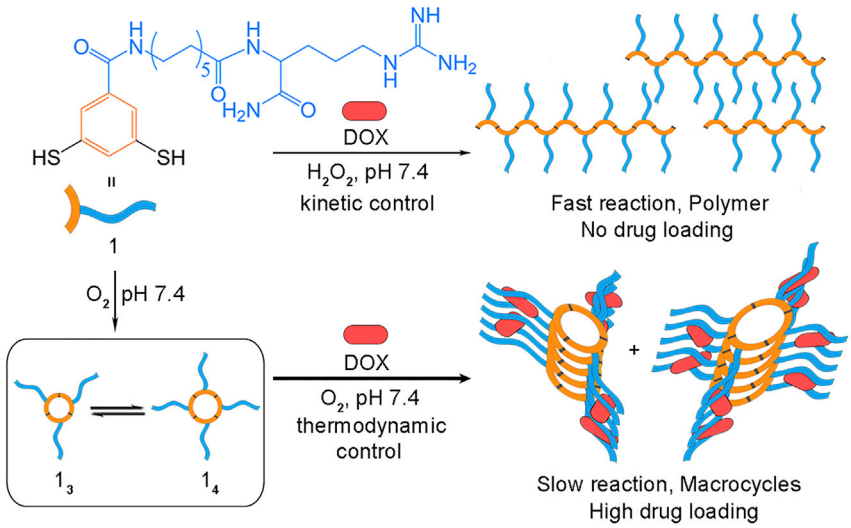

Scheme 1. Schematic illustration of dynamic covalent macrocycle for the co-delivery system showing strong drug-loading capacity under thermodynamic control

However, a polymer made from the same monomer under kinetic control could not load the same drug.

to be equipped with hydrophobic moieties that help the encapsulation of hydrophobic drug molecules and remove the toxic organic solvent at the end of the synthesis.[26] However, the yield of macrocycles is often low owing to the competition reaction between ring closure and chain formation.[27–29] Disulfide bonds are ubiquitous in biological systems and have been proven efficient linkages for the formation of macrocycles.[30–32] Dithiol building blocks in physiological solutions can be oxidized into disulfide macrocycles in the air at room temperature with a quantitative production, when the concentration of the building block is in a millimolar range. As disulfide bonds are also redox responsive, supramolecular nanomaterials self-assembled by disulfide macrocycles are assumed to be disassembled, thereby releasing the loaded drug and gene after endocytosis in cancer cells.[30,33,34] These result from the high concentration of reductants such as glutathione (GSH) inside the cancer cells.[35,36]

Herein, we show the first example of using dynamic covalent macrocycles to explore a gene and drug co-delivery system against drug-resistant cancer (Scheme 1). Macrocycles are spontaneously synthesized from a dithiol building block while associating with a drug molecule non-covalently (see supplemental experimental procedures for details of the synthesis). As the thiol/disulfide exchange reaction continues during a slowly oxidative synthesis, the formation of the macrocycles is reversible, and the final concentration distribution of the macrocycles is under thermodynamic control. Only the macrocycles stabilizing the encapsulation of the drug molecules into self-assembled nanostructures are formed. Such a one-pot strategy integrates the synthesis, self-assembly, and encapsulation procedures into a single step, resulting in a co-delivery system with a high drug-loading content. The as-prepared macrocycles and the drug co-self-assemble into nanofibers. Through ionic interactions with siRNA, the nanofibers are subsequently kneaded into nanoballs. The resulting material shows controlled release of siRNA and the drug in different conditions, good biocompatibility, strong stability, and synergistic therapeutic effects against MDR in tumor cells. However, in a control group, a disulfide polymer is prepared from the same building block in a significantly accelerated oxidation process. The

polymer has an extremely low drug-loading content. These findings suggest that the responsive macrocycles show enhanced drug-loading capacity compared with the corresponding polymer. The one-pot strategy for synthesizing the macrocycle mediated by dynamic covalent chemistry (DCC) provides a new possibility toward efficient synergistic delivery systems meeting clinical needs.

RESULTS AND DISCUSSION

Synthesis and characterization of 1_3 + 1_4/DOX nanofibers

First, we synthesized a dithiol building block **1** by attaching a hydrophobic segment functionalized with an arginine to a 3,5-dimercaptobenzoic acid. The hydrophobic segment was supposed to encapsulate a drug molecule owing to hydrophobic effects. The positive charge of the arginine moiety would help siRNA loading through ionic interactions and improve the cell penetration and nuclear localization of the target nanocarriers. Together with building block **1**, doxorubicin (DOX), a typical anti-cancer drug, and siRNA against drug resistance were chosen for the construction of a responsive macrocycle co-delivery system. Although DOX has been widely used for cancer treatment, its clinical outcome remains unsatisfactory because of the negative effects caused MDR. One of the most significant underlying mechanisms of MDR relates to two types of membrane transport proteins: P-glycoprotein (P-gp) and MDR-associated proteins.[2,37] These proteins can efflux anti-cancer drugs out of cells or cell organelles, decreasing the intracellular drug concentration and the efficacy of the drugs.[38] Therefore, to overcome drug resistance, we loaded anti-P-gp siRNA, which can inhibit the expression of pump proteins and maintain the concentration of DOX at an effective level.[6,39]

Subsequently, the **1** (0.4 mM) was used to prepare a delivery system (1_3 + 1_4/DOX) with the DOX (0.25 mM) in phosphate-buffered saline (PBS) buffer (pH 7.4). The solution was cloudy once it was mixed but gradually became clear after 7 days. The component analysis of the mixture after dialysis using high-performance liquid chromatography-mass spectrometry (HPLC-MS) showed that the **1** was mainly oxidized into trimeric (1_3) and tetrameric (1_4) macrocycles in the air (Figures 1A and S7–S9). In addition, the two macrocycles were also characterized in deuterated dimethyl sulfoxide using ^{1}H nuclear magnetic resonance (NMR) (Figure S10). The drug-loading content (DLC) of the delivery system was approximately 30.2%. However, in a control experiment, by accelerating the oxidation of the **1** (0.4 mM) in the same solution using hydrogen peroxide, the mixture was colorless after dialysis, which indicated that the DOX was not loaded. Moreover, a broad peak was observed in the HPLC spectra of the sample (Figure 1A), while the peak corresponding to the original **1** appeared when excessive amounts of reductant dithiothreitol (DTT) were added (Figure S11). The HPLC analysis was similar to our previous findings. The kinetic control over the dithiol oxidation led to the formation of disulfide polymer from the **1**. With the addition of DTT, the polymer was reduced to **1**. These results demonstrated that, different from the most reported examples that have explored delivery systems using a specific known macrocycle,[21,40,41] the **1** was actually a reactant that produced the self-assembling macrocycles with the DOX during the slowly oxidative process. Thermodynamics directed the synthesis of the right self-assembling macrocycles that can efficiently encapsulate the DOX molecules, giving rise to a high DLC.

The morphology of the nanostructures in the 1_3 + 1_4/DOX system was further examined using transmission electron microscopy (TEM). The macrocycles (1_3 and 1_4) and DOX co-self-assembled into nanofibers with a diameter of approximately 6 nm (Figures 1B and S12C), which was nearly identical to the size (approximately

Please cite this article in press as: Lyu et al., Dynamic covalent macrocycles co-delivering genes and drugs against drug-resistant cancer, Cell Reports Physical Science (2022), https://doi.org/10.1016/j.xcrp.2022.101150

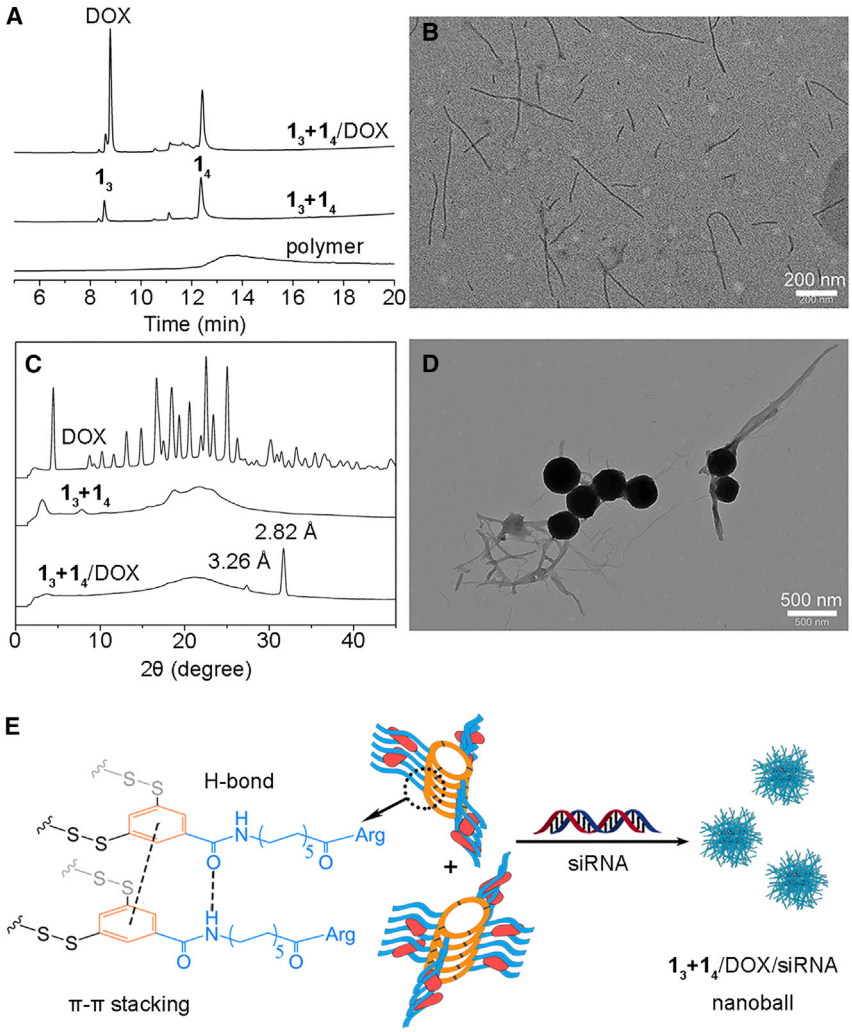

Figure 1. Characterization of 1_3 + 1_4/DOX nanofiber and 1_3 + 1_4/DOX/siRNA nanoball formation

(A) HPLC analysis of 1_3 + 1_4/DOX, 1_3 + 1_4 and polymer oxidized by H_2O_2 in PBS buffer (pH 7.4).

(B) TEM analysis of 1_3 + 1_4/DOX nanofibers. Scale bar, 200 nm.

(C) PXRD of DOX, 1_3 + 1_4, and 1_3 + 1_4/DOX.

(D) TEM analysis of 1_3 + 1_4/DOX/siRNA nanoballs. Scale bar, 500 nm.

(E) Schematic illustration for the non-covalent interaction for organizing nanofibers and the formation of 1_3 + 1_4/DOX/siRNA nanoballs.

4.8 nm) of the macrocycles determined by Chem3D (Figure S13), suggesting that the macrocycles stacked into fibers. Moreover, the analysis of the powder X-ray diffraction (PXRD) data of 1_3+1_4/DOX revealed that a semi-crystalline nature appeared. In Figure 1C, the new peak at 27.33° corresponded to the π-π stacking distance of 3.26 Å between macrocycles, and the new peak at 31.70° resulted from the interaction of the hydrophobic chains in macrocycles.[42] Furthermore, the signal of DOX in the spectra almost disappeared, indicating that DOX was fully encapsulated as non-crystalline within the nanofibers. These results demonstrate that the involvement of DOX aligned the arrangement of the macrocycles. Considering the amphiphilicity of DOX, we propose that DOX molecules may be buried in the hydrophobic branches of the macrocycles but adjacent to the arginine moiety. Apart from the π-π interaction, hydrogen bonding between the amide groups was also crucial to organizing the nanofibers. In the Fourier-transform infrared spectrum of 1_3 + 1_4, the absorption

peaks at 1,631 cm^{-1} belonged to the carbonyl peaks of macrocycles, and the peaks at 1,548 cm^{-1} were assigned to the N–H groups (Figure S14). After loading DOX, the absorption bonds of the C=O and N–H groups of macrocycles moved to 1,620 and 1,538 cm^{-1}, respectively, confirming that hydrogen bonds form between DOX and the hydrophobic branches of the macrocycles in 1_3 + 1_4/DOX system. Thus, the organization of the components at the molecular level into nanofibers is summarized in Figure 1E.[43–45]

Synthesis and characterization of the co-delivery system

We continued to load the siRNA to the 1_3 + 1_4/DOX nanofibers to make the co-delivery system. As the main interaction for loading siRNA was the ionic interaction between the guanidine and the phosphate groups, and as their ratio would play a significant role in the loading process, various ratios between the 1_3 + 1_4/DOX mixture and siRNA were co-incubated. As illustrated in Figure S15A, when the N/P ratio was higher than 4, the 1_3 + 1_4/DOX completely retarded the siRNA migration, demonstrating the full complexation of the negatively charged siRNA chains. Moreover, the loading stability was also investigated by conducting a competition experiment. In the human body, the presence of polyanions may compete with siRNA for binding with nanoparticles, resulting in the desorption of siRNA. In a heparin decomplexation assay (Figure S15B), when the N/P ratio was $\geq$6, the 1_3 + 1_4/DOX loaded with siRNA (1_3 + 1_4/DOX/siRNA) could withstand the replacement of the anionic heparin. Therefore, considering that excessive amounts of siRNA may cause side effects to normal cells, we regarded the optimized N/P ratio as 6 for a stable 1_3 + 1_4/DOX/siRNA system.

With this ratio, fluorescently labeled siRNA (FAM-siRNA) allowed us to determine its encapsulation efficiency of 80.7%, which suggests good siRNA-loading performance. The TEM analysis of the loaded sample showed that the previous 1_3 + 1_4/DOX nanofibers were kneaded into nanoballs with the average size of approximately 260 nm, which was in agreement with the Z-average size in dynamic light scattering (DLS) analysis (Figures 1D and 1E; Table S1). In addition, the PXRD analysis of 1_3 + 1_4/DOX/siRNA nanoparticles was almost the same as that of 1_3 + 1_4/DOX nanofibers, suggesting that the addition of siRNA had little influence on the molecular arrangement of the macrocycles and DOX (Figure S16). Compared with 1_3 + 1_4/DOX nanofibers, 1_3 + 1_4/DOX/siRNA nanoballs had a decrease in polydispersity index (PDI) value in DLS data, which indicates that the nanoparticles had a better uniformity than the nanofibers with different lengths. Besides, the zeta potential of the 1_3 + 1_4/DOX nanofibers was 17.70 $\pm$ 0.61 mV, revealing that the nanostructure was positively charged. With a small loading amount of siRNA with negative charges, the zeta potential of the resulting 1_3 + 1_4/DOX/siRNA nanoballs was slightly decreased to 16.93 $\pm$ 0.06 mV, which verified that the co-delivery system was stabilized by ionic interaction (Table S1).

Redox- and pH-induced release of DOX and siRNA from the co-delivery system

Once the 1_3 + 1_4/DOX/siRNA system was obtained, we proceeded to test its responsiveness. In general, environmental changes can trigger well-organized nanoparticles to disassemble and thereby release the loaded target. For the 1_3 + 1_4/DOX/siRNA system, we considered pH and redox stimuli for the release. The tumor microenvironment is more acid than normal tissues,[46] which protonated the phosphate group of siRNA, weakening the ionic interaction between siRNA and the macrocycles. In addition, the concentration of GSH in cancer cells (>5 mM) is much higher than that in extracellular matrices at tumors sites.[36,47] This can reduce the disulfide bonds of the 1_3 + 1_4 macrocycles into building block 1, breaking the nanostructure and releasing the drug and gene. Thus, these dual stimuli were applied to simulate the biological and endo-lysosomal environments for

Please cite this article in press as: Lyu et al., Dynamic covalent macrocycles co-delivering genes and drugs against drug-resistant cancer, Cell Reports Physical Science (2022), https://doi.org/10.1016/j.xcrp.2022.101150

monitoring the release profile of DOX and the gene siRNA *in vitro*. As shown in Figure S17A, the cumulative DOX release profile was <6% at pH 7.4, indicating the 1_3 + 1_4/DOX/siRNA nanoballs were stable in the normal environment. The release of DOX from the 1_3 + 1_4/DOX/siRNA at endo-lysosomal pH 5.5 in the presence of GSH was much faster than that at a physiological pH of 7.4. Within 12 h, approximately 60% of the total DOX in the nanoballs was released, while the cumulative leakage was <7% within the same period at pH 5.5 without GSH. In addition, to determine whether DOX and siRNA could be released into the medium at the same time, the FAM-siRNA released from the nanoballs was also investigated using a fluorescent spectrometer. In Figure S17B, a similar release behavior could be observed at different conditions. On the basis of these results, the 1_3 + 1_4/DOX/siRNA nanoballs were stable in circulation but could have a rapid release behavior in the reductive acid tumor environment. This characteristic would reduce the systemic toxicity of DOX, increase drug accumulation in the cytoplasm of tumor cells, and facilitate drug and siRNA co-anti-tumor activity.[48]

Blood compatibility

Then, a hemolytic study was conducted to evaluate responses arising between nanoparticles and blood components, which could assess the safety and biocompatibility of the 1_3 + 1_4/DOX/siRNA system. As shown in Figure S18, the 1_3 + 1_4/DOX/siRNA system exhibited <5% hemolytic activity in red blood cells even at the highest DOX concentration of 8 mg/mL, which demonstrated that the 1_3 + 1_4/DOX/siRNA co-delivery system showed excellent blood compatibility and suitability for intravenous administration of the co-delivery system.

Enhanced cellular uptake of the co-delivery system

Next, the ability of the 1_3 + 1_4/DOX/FAM-siRNA system to deliver DOX and siRNA into drug-resistant NCI/ADR-RES cells were confirmed using confocal laser scanning microscopy and flow cytometry. As shown in Figure 2A, FAM-siRNAs were delivered into cells at extremely high cellular uptake levels through the endocytosis of 1_3 + 1_4/DOX/FAM-siRNA, compared with the naked FAM-siRNA group, which was attributed to the high surface charge of the nanoballs that could increase the interaction between the carrier and the cell membrane. Similarly, the DOX signal intensity of 1_3 + 1_4/DOX/FAM-siRNA was significantly higher than that of the free DOX group, which confirmed that DOX had partly and effectively entered the nuclei (Figures 2A and 2B). These results suggest that the macrocycle system could efficiently deliver siRNA and DOX into NCI/ADR-RES cells. Previous reports have shown that P-gp plays an important role in the development of drug resistance, as it effectively pumps out administered drugs.[37] To investigate whether 1_3 + 1_4/DOX/siRNA could effectively deliver anti-P-gp siRNA into NCI/ADR-RES cells, cells were incubated with 1_3 + 1_4/DOX/siRNA, and then P-gp expression was detected using a western blotting assay. As shown in Figure 2C, no obvious downregulation of P-gp expression was found for the free P-gp siRNA group, indicating that P-gp siRNA was not sufficiently internalized into NCI/ADR-RES cells. By contrast, a significant downregulation of P-gp expression was observed in the 1_3 + 1_4/DOX/siRNA group, indicating that 1_3 + 1_4/DOX/siRNA can efficiently deliver P-gp siRNA into NCI/ADR-RES cells and can be transfected, resulting in a downregulation of P-gp expression. Thus, 1_3 + 1_4/DOX/siRNA systems may offer enhanced MDR cell killing by inducing synergistic therapeutic effects.

In vitro cytotoxicity and fighting against drug-resistant tumors of the co-delivery system

Finally, to evaluate the synergistic potential of 1_3 + 1_4/DOX/siRNA co-delivery systems against NCI/ADR-RES cells, the *in vitro* cytotoxicity levels of free DOX, free

Please cite this article in press as: Lyu et al., Dynamic covalent macrocycles co-delivering genes and drugs against drug-resistant cancer, Cell Reports Physical Science (2022), https://doi.org/10.1016/j.xcrp.2022.101150

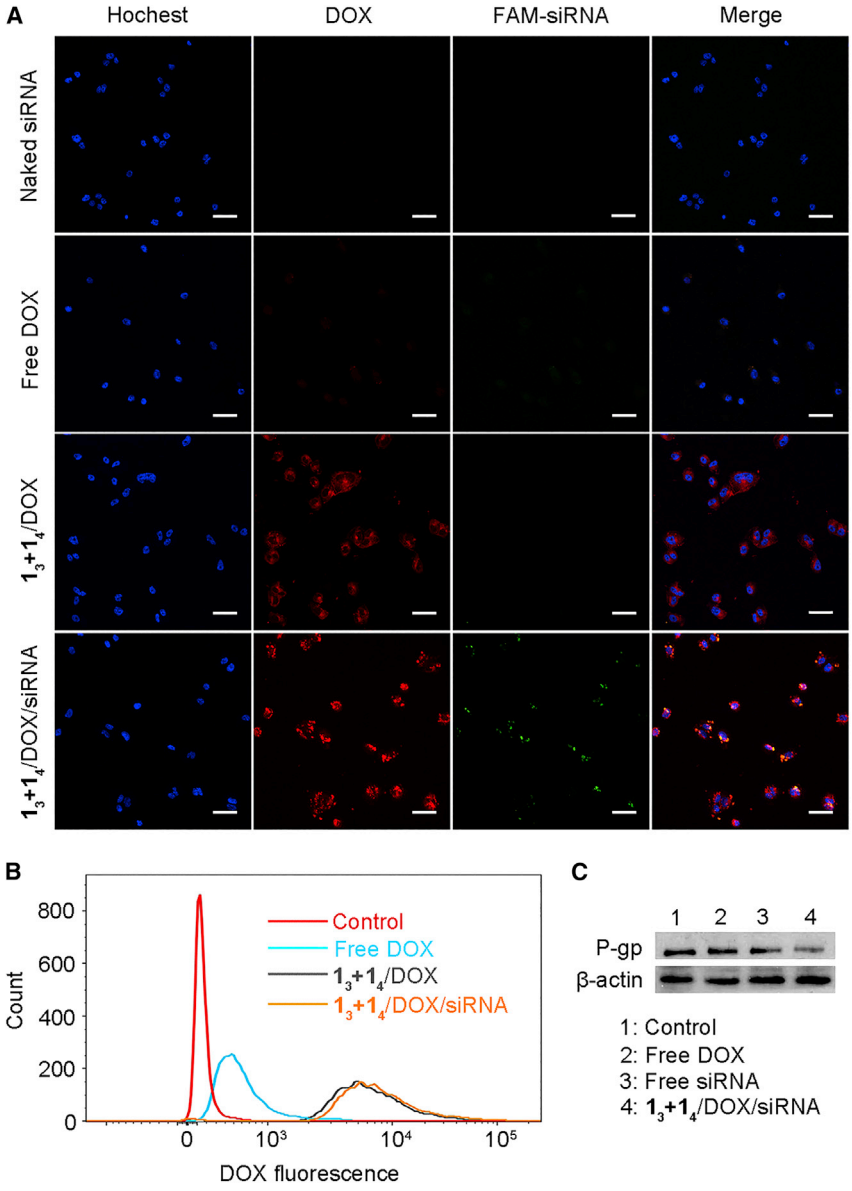

Figure 2. Cell uptake studies of 1_3 + 1_4/DOX/siRNA co-delivery system

(A) Fluorescence microscopy images of NCI/ADR-RES cells incubated with different formulations. Green, red, and blue fluorescence indicate FAM-siRNA, DOX, and the nucleus, respectively. Scale bar, 50 μm.

(B) Flow cytometry of the NCI/ADR-RES cells incubated with different formulations.

(C) Western blotting assay of the P-gp expression against different formulations in NCI/ADR-RES cells.

siRNA, 1_3 + 1_4/DOX, and 1_3 + 1_4/DOX/siRNA were evaluated in NCI/ADR-RES cells using an MTT assay. As shown in Figure 3A, the cell viability of NCI/ADR-RES cells dramatically decreased after treatment with 1_3 + 1_4/DOX, whereas free DOX had a much lower effect, indicating that the nanofibers could increase the cell uptake of the anti-tumor agent into the cytoplasm. When the DOX concentration was high, the cell viability of NCI/ADR-RES cells incubated with 1_3 + 1_4/DOX/siRNA decreased to 21.6%, which could be attributed to the delivery of DOX and siRNA into the cytoplasm to exert their synergistic anti-tumor effect. Moreover, as shown

Please cite this article in press as: Lyu et al., Dynamic covalent macrocycles co-delivering genes and drugs against drug-resistant cancer, Cell Reports Physical Science (2022), https://doi.org/10.1016/j.xcrp.2022.101150

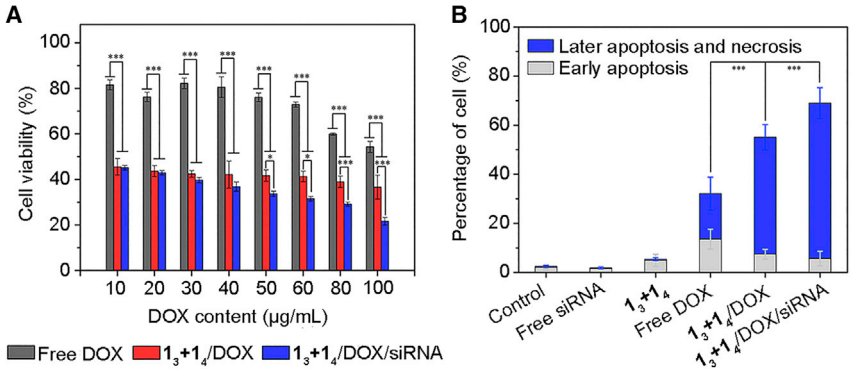

Figure 3. *In vitro* cytotoxicity and apoptosis assay

(A) *In vitro* anticancer efficacy. NCI/ADR-RES cells were incubated with different formulations.

(B) Percentage of NCI/ADR-RES cells in different stages from apoptosis assay after being treated with different formulations.

All of the measurements were performed at least in triplicate; error bars represent SDs about the mean. *$p < 0.05$, **$p < 0.01$, and ***$p < 0.001$.

in Figures S19 and S20, no significant cytotoxicity against NCI/ADR-RES cells and HEK293 cells was observed for macrocycles (1_3 + 1_4) at concentrations of up to 0.2 mM, indicating that macrocycles showed good biocompatibility, which may be due to the presence of an arginine group.[49] Furthermore, in the non-MDR (MCF-7S) cells, which do not actively pump out DOX, 1_3 + 1_4/DOX and 1_3 + 1_4/DOX/siRNA had similar cytotoxicity levels, which were higher than that of free DOX (Figure S21).

To confirm the anti-tumor effect of the 1_3 + 1_4/DOX/siRNA system, we used fluorescein-isothiocyanate-labeled annexin V and propidium iodide to stain NCI/ADR-RES cells treated with different formulations to determine their apoptotic efficiency. As shown in Figures 3B and S22, the NCI/ADR-RES cells in the 1_3 + 1_4/DOX/siRNA group exhibited higher levels of later apoptosis and necrosis (63.3%) than those in the 1_3 + 1_4/DOX (47.6%) and free DOX groups (6.8%). The results could be attributed to the fact that the suppression of P-gp efflux pumps in NCI/ADR-RES cells by P-gp siRNA will lead to an increase in intracellular drug concentration and induce cell apoptosis. We also found that the 1_3 + 1_4 group had low cytotoxicity on NCI/ADR-RES cells, similarly to free siRNA. These results further confirmed that 1_3 + 1_4/DOX/siRNA could co-deliver DOX and P-gp siRNA into NCI/ADR-RES cells and increase anti-tumor efficacy.

In summary, we have employed DCC to construct a responsive macrocycle co-delivery system that delivers drug and gene to targeted MDR cancer cells. The thermodynamic control behind the principle of DCC was crucial to enhance the loading capacity of the delivery system. Under a slow reaction rate, the dynamic system had ample time to allow the thiol/disulfide exchange reaction to take place and reach an equilibrium, which resulted in the production of the macrocycle carriers and a high DLC. However, when the reaction was significantly accelerated, disulfide polymers were obtained from the same monomer, but they were not able to encapsulate the drug. The utility of our macrocycle system was demonstrated by further loading a functional gene, and the resulting co-delivery system displayed the controllable release of drug and gene, as well as improved synergistic efficacy against NCI/ADR-RES cells *in vitro*. We expect that our macrocycle co-delivery system explored by the strategy of DCC could serve as a versatile nanocarrier for drug and gene co-delivery to target a broad range of diseases.

Cell Reports
Physical Science
Report

EXPERIMENTAL PROCEDURES

Resource availability

Lead contact

Further information and requests for resources and reagents should be directed to and will be fulfilled by the lead contact, Dr. Jianwei Li (jianwei.li@utu.fi).

Materials availability

All stable and unique materials generated in this study are available from the lead contact upon reasonable request.

Data and code availability

All of the data supporting this study have been shown in the article and supplemental information. Other related data are available from the corresponding authors upon reasonable request.

SUPPLEMENTAL INFORMATION

Supplemental information can be found online at https://doi.org/10.1016/j.xcrp.2022.101150.

ACKNOWLEDGMENTS

We are grateful for the financial support from the Sigrid Jusélius Foundation (starting grant for J.L.), the Academy of Finland (decision no. 318524, project funding for J.L.), the Finnish Cultural Foundation (PhD fellowship for Y.L.), and the China Scholarship Council (PhD scholarships for J.Y. and X.W.). We thank Turku Center for Chemical and Molecular Analytics for providing NMR and LC-MS technology and the Electron Microscopy Laboratory, Institute of Biomedicine, University of Turku, and Biocenter Finland for TEM imaging. A.C.P. thanks Biocenter Finland for infrastructure support. We thank Prof. M. Vilanova (Universitat de Girona, Spain) for her generous donation of the NCI/ADR-RES cells and D. Eichin and V. Viloma for giving guidance on the gene expression part.

AUTHOR CONTRIBUTIONS

Y.L. conceived the idea, carried out the synthesis, characterization, and cell experiments, and wrote the manuscript. X.W. helped with cell experiments. A.C.P. carried out the PXRD characterization. J.Y. and X.W. carried out part of the synthesis. D.Q. gave the suggestion on drawing figures. J.L. supervised the research and wrote the paper.

DECLARATION OF INTERESTS

The authors declare no competing interests.

Received: July 22, 2022
Revised: September 19, 2022
Accepted: October 19, 2022
Published: November 9, 2022

REFERENCES

1. Szakács, G., Paterson, J.K., Ludwig, J.A., Booth-Genthe, C., and Gottesman, M.M. (2006). Targeting multidrug resistance in cancer. Nat. Rev. Drug Discov. *5*, 219–234. https://doi.org/10.1038/nrd1984.

2. Saraswathy, M., and Gong, S. (2013). Different strategies to overcome multidrug resistance in cancer. Biotechnol. Adv. *31*, 1397–1407. https://doi.org/10.1016/j.biotechadv.2013.06.004.

3. Kathawala, R.J., Gupta, P., Ashby, C.R., Jr., and Chen, Z.S. (2015). The modulation of ABC transporter-mediated multidrug resistance in cancer: a review of the past decade. Drug Resist. Updat. *18*, 1–17. https://doi.org/10.1016/j.drup.2014.11.002.

4. Ye, Q., Liu, K., Shen, Q., Li, Q., Hao, J., Han, F., and Jiang, R.W. (2019). Reversal of multidrug resistance in cancer by multi-functional flavonoids. Front. Oncol. *9*, 487. https://doi.org/10.3389/fonc.2019.00487.

5. Caetano-Pinto, P., Jansen, J., Assaraf, Y.G., and Masereeuw, R. (2017). The importance of breast cancer resistance protein to the kidneys excretory function and chemotherapeutic resistance. Drug Resist. Updat. *30*, 15–27. https://doi.org/10.1016/j.drup.2017.01.002.

6. Iorns, E., Lord, C.J., Turner, N., and Ashworth, A. (2007). Utilizing RNA interference to enhance cancer drug discovery. Nat. Rev. Drug Discov. *6*, 556–568. https://doi.org/10.1038/nrd2355.

7. Liu, H., Li, Y., Mozhi, A., Zhang, L., Liu, Y., Xu, X., Xing, J., Liang, X., Ma, G., Yang, J., and Zhang, X. (2014). SiRNA-phospholipid conjugates for gene and drug delivery in cancer treatment. Biomaterials *35*, 6519–6533. https://doi.org/10.1016/j.biomaterials.2014.04.033.

8. Du, J., Shao, Y., Hu, Y., Chen, Y., Cang, J., Chen, X., Pei, W., Miao, F., Shen, Y., Muddassir, M., et al. (2021). Multifunctional liposomes enable active targeting and twinfilin 1 silencing to reverse paclitaxel resistance in brain metastatic breast cancer. ACS Appl. Mater. Interfaces *13*, 23396–23409. https://doi.org/10.1021/acsami.1c02822.

9. Pan, Q.S., Chen, T.T., Nie, C.P., Yi, J.T., Liu, C., Hu, Y.L., and Chu, X. (2018). In situ synthesis of ultrathin ZIF-8 film-coated MSNs for codelivering Bcl 2 siRNA and doxorubicin to enhance chemotherapeutic efficacy in drug-resistant cancer cells. ACS Appl. Mater. Interfaces *10*, 33070–33077. https://doi.org/10.1021/acsami.8b13393.

10. Zhang, S., Chen, C., Xue, C., Chang, D., Xu, H., Salena, B.J., Li, Y., and Wu, Z.S. (2020). Ribbon of DNA lattice on gold nanoparticles for selective drug delivery to cancer cells. Angew. Chem. Int. Ed. Engl. *59*, 14584–14592. https://doi.org/10.1002/anie.202005624.

11. Bognanni, N., Viale, M., Distefano, A., Tosto, R., Bertola, N., Loiacono, F., Ponassi, M., Spinelli, D., Pappalardo, G., and Vecchio, G. (2021). Cyclodextrin polymers as delivery systems for targeted anti-cancer chemotherapy. Molecules *26*, 6046. https://doi.org/10.3390/molecules26196046.

12. Cheng, Q., Du, L., Meng, L., Han, S., Wei, T., Wang, X., Wu, Y., Song, X., Zhou, J., Zheng, S., et al. (2016). The promising nanocarrier for doxorubicin and siRNA co-delivery by PDMAEMA-based amphiphilic nanomicelles. ACS Appl. Mater. Interfaces *8*, 4347–4356. https://doi.org/10.1021/acsami.5b11789.

13. Yang, X.Z., Dou, S., Wang, Y.C., Long, H.Y., Xiong, M.H., Mao, C.Q., Yao, Y.D., and Wang, J. (2012). Single-step assembly of cationic lipid polymer hybrid nanoparticles for systemic delivery of siRNA. ACS Nano *6*, 4955–4965. https://doi.org/10.1021/nn300500u.

14. Knop, K., Hoogenboom, R., Fischer, D., and Schubert, U.S. (2010). Poly(ethylene glycol) in drug delivery: pros and cons as well as potential alternatives. Angew. Chem. Int. Ed. Engl. *49*, 6288–6308. https://doi.org/10.1002/anie.200902672.

15. Coelho, J.F., Ferreira, P.C., Alves, P., Cordeiro, R., Fonseca, A.C., Góis, J.R., and Gil, M.H. (2010). Drug delivery systems: advanced technologies potentially applicable in personalized treatments. EPMA J. *1*, 164–209. https://doi.org/10.1007/s13167-010-0001-x.

16. Patra, J.K., Das, G., Fraceto, L.F., Campos, E.V.R., Rodriguez-Torres, M.D.P., Acosta-Torres, L.S., Diaz-Torres, L.A., Grillo, R., Swamy, M.K., Sharma, S., et al. (2018). Nano based drug delivery systems: recent developments and future prospects. J. Nanobiotechnol. *16*, 71. https://doi.org/10.1186/s12951-018-0392-8.

17. Barenholz, Y. (2012). Doxil(R)-the first FDA-approved nano-drug: lessons learned. J. Contr. Release *160*, 117–134. https://doi.org/10.1016/j.jconrel.2012.03.020.

18. Jain, R.K., and Stylianopoulos, T. (2010). Delivering nanomedicine to solid tumors. Nat. Rev. Clin. Oncol. *7*, 653–664. https://doi.org/10.1038/nrclinonc.2010.139.

19. Tejada-Berges, T., Granai, C.O., Gordinier, M., and Gajewski, W. (2002). Caelyx/Doxil for the treatment of metastatic ovarian and breast cancer. Expert Rev. Anticancer Ther. *2*, 143–150. https://doi.org/10.1586/14737140.2.2.143.

20. Ren, C., Liu, H., Lv, F., Zhao, W., Gao, S., Yang, X., Jin, Y., Tan, Y., Zhang, J., Liang, X.J., and Li, Z. (2020). Prodrug-based nanoreactors with tumor-specific *in situ* activation for multisynergistic cancer therapy. ACS Appl. Mater. Interfaces *12*, 34667–34677. https://doi.org/10.1021/acsami.0c09489.

21. Liu, Q., Zhang, T.X., Zheng, Y., Wang, C., Kang, Z., Zhao, Y., Chai, J., Li, H.B., Guo, D.S., Liu, Y., and Shi, L. (2021). Calixarene-embedded nanoparticles for interference-free gene-drug combination cancer therapy. Small *17*, 2006223. https://doi.org/10.1002/smll.202006223.

22. Bai, H., Wang, J., Li, Z., and Tang, G. (2019). Macrocyclic compounds for drug and gene delivery in immune-modulating therapy. Int. J. Mol. Sci. *20*, 2097. https://doi.org/10.3390/ijms20092097.

23. Sigwalt, D., Holler, M., Iehl, J., Nierengarten, J.F., Nothisen, M., Morin, E., and Remy, J.S. (2011). Gene delivery with polycationic fullerene hexakis-adducts. Chem. Commun. *47*, 4640–4642. https://doi.org/10.1039/C0CC05783E.

24. Nakai, T., Kanamori, T., Sando, S., and Aoyama, Y. (2003). Remarkably size-regulated cell invasion by artificial viruses. saccharide-dependent self-aggregation of glycoviruses and its consequences in glycoviral gene delivery. J. Am. Chem. Soc. *125*, 8465–8475. https://doi.org/10.1021/ja035636f.

25. Xiao, T., Qi, L., Zhong, W., Lin, C., Wang, R., and Wang, L. (2019). Stimuli-responsive nanocarriers constructed from pillar[n]arene-based supra-amphiphiles. Mater. Chem. Front. *3*, 1973–1993. https://doi.org/10.1039/C9QM00428A.

26. Ostos, F.J., Lebrón, J.A., López-Cornejo, P., López-López, M., García-Calderón, M., García-Calderón, C.B., Rosado, I.V., Kalchenko, V.I., Rodik, R.V., and Moyá, M.L. (2020). Self-aggregation in aqueous solution of amphiphilic cationic calix[4]arenes. Potential use as vectors and nanocarriers. J. Mol. Liq. *304*, 112724. https://doi.org/10.1016/j.molliq.2020.112724.

27. Zhang, S., and Zhao, L. (2018). Macrocycle-encircled polynuclear metal clusters: controllable synthesis, reactivity studies, and applications. Acc. Chem. Res. *51*, 2535–2545. https://doi.org/10.1021/acs.accounts.8b00283.

28. Sánchez-García, D., and Sessler, J.L. (2008). Porphycenes: synthesis and derivatives. Chem. Soc. Rev. *37*, 215–232. https://doi.org/10.1039/B704945E.

29. Zhu, H., Shangguan, L., Shi, B., Yu, G., and Huang, F. (2018). Recent progress in macrocyclic amphiphiles and macrocyclic host-based supra-amphiphiles. Mater. Chem. Front. *2*, 2152–2174. https://doi.org/10.1039/C8QM00314A.

30. Wang, M., and Jiang, X. (2018). Sulfur-sulfur bond construction. Top. Curr. Chem. *376*, 14. https://doi.org/10.1007/s41061-018-0192-5.

31. Pal, A., Malakoutikhah, M., Leonetti, G., Tezcan, M., Colomb-Delsuc, M., Nguyen, V.D., van der Gucht, J., and Otto, S. (2015). Controlling the structure and length of self-synthesizing supramolecular polymers through nucleated growth and disassembly. Angew. Chem. Int. Ed. Engl. *54*, 7852–7856. https://doi.org/10.1002/ange.201501965.

32. Li, J., Nowak, P., and Otto, S. (2013). Dynamic combinatorial libraries: from exploring molecular recognition to systems chemistry. J. Am. Chem. Soc. *135*, 9222–9239. https://doi.org/10.1021/ja402586c.

33. Lee, M.H., Yang, Z., Lim, C.W., Lee, Y.H., Dongbang, S., Kang, C., and Kim, J.S. (2013). Disulfide-cleavage-triggered chemosensors and their biological applications. Chem. Rev. *113*, 5071–5109. https://doi.org/10.1021/cr300358b.

34. Cao, Y., Yang, J., Eichin, D., Zhao, F., Qi, D., Kahari, L., Jia, C., Peurla, M., Rosenholm, J.M., Zhao, Z., et al. (2021). Self-synthesizing nanorods from dynamic combinatorial libraries against drug resistant cancer. Angew. Chem. Int. Ed. Engl. *60*, 3062–3070. https://doi.org/10.1002/anie.202010937.

35. Estrela, J.M., Ortega, A., and Obrador, E. (2006). Glutathione in cancer biology and therapy. Crit. Rev. Clin. Lab Sci. *43*, 143–181. https://doi.org/10.1080/10408360500523878.

36. Bansal, A., and Simon, M.C. (2018). Glutathione metabolism in cancer progression and treatment resistance. J. Cell Biol. *217*, 2291–2298. https://doi.org/10.1083/jcb.201804161.

37. Saneja, A., Khare, V., Alam, N., Dubey, R.D., and Gupta, P.N. (2014). Advances in P-glycoprotein-based approaches for delivering anticancer drugs: pharmacokinetic perspective and clinical relevance. Expert Opin. Drug Deliv. *11*, 121–138. https://doi.org/10.1517/17425247.2014.865014.

38. Li, W., Zhang, H., Assaraf, Y.G., Zhao, K., Xu, X., Xie, J., Yang, D.H., and Chen, Z.S. (2016). Overcoming ABC transporter-mediated multidrug resistance: molecular mechanisms and novel therapeutic drug strategies. Drug Resist. Updat. *27*, 14–29. https://doi.org/10.1016/j.drup.2016.05.001.

39. Shahabipour, F., Barati, N., Johnston, T.P., Derosa, G., Maffioli, P., and Sahebkar, A. (2017). Exosomes: nanoparticulate tools for RNA

interference and drug delivery. J. Cell. Physiol. *232*, 1660–1668. https://doi.org/10.1002/jcp.25766.

40. Kashapov, R.R., Razuvayeva, Y.S., Ziganshina, A.Y., Mukhitova, R.K., Sapunova, A.S., Voloshina, A.D., Nizameev, I.R., Kadirov, M.K., and Zakharova, L.Y. (2020). Design of *N*-methyl-$_D$-glucamine-based resorcin[4]arene nanoparticles for enhanced apoptosis effects. Mol. Pharm. *17*, 40–49. https://doi.org/10.1021/acs.molpharmaceut.9b00599.

41. Shen, J., Wang, Q., Hu, Q., Li, Y., Tang, G., and Chu, P.K. (2014). Restoration of chemosensitivity by multifunctional micelles mediated by P-gp siRNA to reverse MDR. Biomaterials *35*, 8621–8634. https://doi.org/10.1016/j.biomaterials.2014.06.035.

42. Aigouy, T., Costeseque, P., Sempere, R., Senac, T., Jaud, J., and Anglerot, D. (1995). Caracterisation structurale et evolution thermique de l'acide amino-11-undecanoique. Acta Crystallogr. B *51*, 55–61. https://doi.org/10.1107/S010876819400159X.

43. Gulmez, F., Yercan, A., Kocaaga, B., and Guner, F.S. (2021). pH-sensitive castor oil/PEG-based polyurethane films for drug delivery. J. Drug Deliv. Sci. Technol. *61*, 102160. https://doi.org/10.1016/j.jddst.2020.102160.

44. Motaali, S., Pashaeiasl, M., Akbarzadeh, A., and Davaran, S. (2017). Synthesis and characterization of smart *N*-isopropylacrylamide-based magnetic nanocomposites containing doxorubicin anti-cancer drug. Artif. Cells Nanomed. Biotechnol. *45*, 560–567. https://doi.org/10.3109/21691401.2016.1161640.

45. Rao, Z., Ge, H., Liu, L., Zhu, C., Min, L., Liu, M., Fan, L., and Li, D. (2018). Carboxymethyl cellulose modified graphene oxide as pH-sensitive drug delivery system. Int. J. Biol. Macromol. *107*, 1184–1192. https://doi.org/10.1016/j.ijbiomac.2017.09.096.

46. Mura, S., Nicolas, J., and Couvreur, P. (2013). Stimuli-responsive nanocarriers for drug delivery. Nat. Mater. *12*, 991–1003. https://doi.org/10.1038/nmat3776.

47. Torchilin, V.P. (2014). Multifunctional, stimuli-sensitive nanoparticulate systems for drug delivery. Nat. Rev. Drug Discov. *13*, 813–827. https://doi.org/10.1038/nrd4333.

48. Li, Y., Thambi, T., and Lee, D.S. (2018). Co-delivery of drugs and genes using polymeric nanoparticles for synergistic cancer therapeutic effects. Adv. Healthc. Mater. *7*, 1700886. https://doi.org/10.1002/adhm.201700886.

49. Lu, S., Morris, V.B., and Labhasetwar, V. (2015). Codelivery of DNA and siRNA via arginine-rich PEI-based polyplexes. Mol. Pharm. *12*, 621–629. https://doi.org/10.1021/mp5006883.

Cell Reports Physical Science, Volume *3*

Supplemental information

Dynamic covalent macrocycles co-delivering genes and drugs against drug-resistant cancer

Yonglei Lyu, Xiaoxia Wu, Anastassios C. Papageorgiou, Jinghui Yang, Xin Wang, Dawei Qi, and Jianwei Li

Supplemental Experimental Procedures

1. Materials and Methods

Arginine, triethylamine (TEA), *N*-Hydroxysuccinimide (NHS), 3-(ethyliminomethyleneamino)-*N*, *N*-dimethyl-propan-1-amine hydrochloride (EDC·HCl), *N*,*N*-Diisopropylethylamine (DIPEA), 11-aminoundecanoic acid, trimethylamine (TEA), 3-(4,5-dimethylthiazol-2-yl)-2,5-diphenyltetrazolium bromide (MTT), glutathione (GSH), dimethylformamide (DMF), dimethyl sulfoxide (DMSO) and dichloromethane (DCM) were obtained from Sigma-Aldrich. Doxorubicin (DOX) (>98%) was provided by Melone Pharmaceutical Co., Ltd (Dalian, China). 2,5-bis(trithyltio)benzoic acid was synthesized according to the previous report. [S1] Annexin V-fluorescein isothiocyanate (AV-FITC), propidium iodide (PI), and fetal bovine serum (FBS) were received from Invitrogen eBioscience. Dulbecco's Modified Essential Medium (DMEM) were purchased from Invitrogen. The siRNA used in this study was synthesized and purified with high-performance liquid chromatography by Shanghai GenePharma Co. Ltd (China), including scramble siRNA, P-gp siRNA, and fluorescence-labeled FAM-siRNA. The sequence of P-gp siRNA sense was as follows: antisense strand of 5′-GCA CUA AAG UAG GAG ACA ATT-3′ and 5′-GCU GAU CUA UCG AUC UUA UTT-3′. The P-gp primary antibody (ab103477) and beta actin secondary antibody were purchased from Origene.

Nuclear Magnetic Resonance Spectroscopy (NMR): ^{1}H and ^{13}C NMR were recorded on a Bruker NMR spectrometer at 500 MHz. The residual solvent peaks were used as internal references.

Mass Spectrometry (ESI-TOF): Mass spectra were recorded on a Bruker Daltonics micrOTOF-Q ESI and a Thermo Fisher Scientific hybrid quadrupole Orbitrap mass spectrometers using direct infusion.

High Performance Liquid Chromatography (HPLC): HPLC analysis were performed on Agilent 1100 systems equipped with a PDA detector. All analyses were performed using a reversed-phase HPLC column (Waters™ C8 Columns). UV absorbance was monitored at 254 nm. Column temperature was kept at 25 °C. Injection volume: 10 µL of a library subjected to a 1:20 dilution in DMSO (5 v% TFA). Method: Eluent flow: 1.0 mL/min; eluent A: HPLC grade acetonitrile (0.1 v% formic acid); eluent B: deionized water (0.1 v% formic acid)

Time (min)	A%	B%
0	5	95
20	95	5
25	95	5
30	5	95

Dynamic light scattering (DLS): DLS measurement was performed on Zetasizer Nano-ZS (Malvern Instruments Ltd., Worcestershire, UK) with a He-Ne ion laser of 633 nm.

Ultraviolet-Vis (UV-Vis) Absorption Spectroscopy: UV/Vis measurement was performed on a Perkin Elmer Lambda 35 UV/Vis spectrometer.

Powder X-ray diffraction (XRD): Powder XRD experiments were conducted using a MicroMax 007 HF X-ray generator equipped with a HyPix-6000HE photon counting detector.

Transmission Electron Microscopy (TEM): The sizes and morphologies of the samples complex in solution were observed by using a JEM 1400 plus transmission electron microscope. The samples were dissolved in distilled water, and then 5.0 μL of each sample was dropped onto copper grids and air-dried at room temperature.

Preparation of 1_3+1_4/DOX nanofibers

DOX (100 mg) was accurately measured and dissolved in 1 mL deionized water. **1** (0.21 mg) was accurately measured and dissolved in pH 7.4 PBS 1 mL, and then DOX solution (2 μL) was introduced into the mixture. After full oxidation, the prepared **1_3+1_4**/DOX nanofibers was purified by dialysis for 1 day. DOX content was determined using a UV-vis spectrophotometer at 480 nm, and the drug-loading content (DLC) of DOX was determined using the following formula:

$$DLC(\%) = \frac{w_{DOX}}{w_{DOX} + w_{1_3+1_4}} \times 100\%$$

w_{DOX} and $w_{1_3+1_4}$ represent the weight of encapsulated DOX and weight of the macrocycles, respectively.

Preparation of 1_3+1_4/DOX/siRNA nanoballs

Typically, 2 mg of **1_3+1_4**/DOX was dissolved in 1 mL PBS and sonication for 10 min. then, **1_3+1_4**/DOX solution were incubated with siRNA for 1 h at different N/P ratios (0, 1, 2, 3, 4, 5, 6, 8, 10, 15, and 20) to form the **1_3+1_4**/DOX/siRNA nanoballs. The N/P ratio represents the molar ratio of nitrogen in **1_3+1_4**/DOX cationic to phosphate in siRNA. To determine the encapsulation efficiency (EE) of **1_3+1_4**/DOX/siRNA, FAM-siRNA was used. The complex solutions at different N/P ratios were added into Amicon Ultra-4 centrifugal filter devices (50 kD, Millipore, Massachusetts) and centrifuged (speed: 5000 rpm, time: 10 min). The solutions after being centrifuged, which contained uncomplexed FAM-siRNA, were collected and quantified by a NanoDrop Spectrophotometer ND-1000 (Ex: 480 nm; Em: 520 nm). The EE of siRNA was determined using the following formula:

$$EE(\%) = \frac{n_{total} - n_{free}}{n_{total}} \times 100\%$$

n_{total} and n_{free}represent the amount of total and uncomplex FAM-siRNA, respectively.

Agarose Gel Electrophoresis Analysis

The **1_3+1_4**/DOX/siRNA nanoballs solutions at different N/P ratios (0, 1, 2, 3, 4, 5, 6, 8, 10, 15, and 20) were sampled in an agarose gel plate (2% (w/v), ethidium bromide (0.5 mg/mL)) which was submerged in an electrophoresis tank filled with an appropriate amount of Tris-acetate-EDTA buffer. The system was running for 20 min at 120 V. Then, a Bio-Rad Imager was used to obtain the visual result.

Resistance to Heparin Replacement

1_3+1_4/DOX/siRNA solutions at different N/P ratios (0, 1, 2, 3, 4, 5, 6, 8, 10, 15, and 20) were mixed with heparin (heparin/siRNA (IU/mg) = 10) for 10 min. After that, the mixtures were incubated at 25 °C for 60 min. Then, the samples were electrophoresed at 120 V for 20 min.

In Vitro Release of 1_3+1_4/DOX/siRNA in Response to pH/Redox Stimuli

Phosphate buffer at different pH (7.4 and 5.5) with/without 5 mM GSH were selected as the media to simulate biological and early/late endosomal conditions. The **1_3+1_4**/DOX/siRNA solutions were added into dialysis bags and put into a conical flask with 10 mL PBS solution at different pH (7.4 and 5.5) with/without 5 mM GSH. The flasks were then placed into a shaking incubator for 72 h at 37 °C. At a scheduled point, the sample was taken out and an equal medium was added. The amount of DOX in the medium was measured and analyzed by UV-vis spectrophotometer at 480 nm. the siRNA released from the **1_3+1_4**/DOX/siRNA was detected with a ND-1000 as described before.

Cell culture

DOX-sensitive breast cancer cell lines MCF-7S and Human embryonic kidney 293 cells line HEK293 were purchased from the American Type Culture Collection (LGC Standards SARL), and the DOX-resistant NCI/ADR-RES human ovarian cancer cell line (formerly MCF-7/ADR) was a generous gift from Prof. Maria Vilanova at the Department of Biology, Universitat de Girona, and Biomedical Research Institute of Girona in Spain, which was originally from Dr. Ramon Colomer of the Institut Català d'Oncologia de Girona, Hospital Universitari de Girona, Spain. The MCF-7S, NCI/ADR-RES and HEK293 cells were all routinely grown at 37°C in a humidified atmosphere of 5% CO_2 in Dulbecco's Modified Eagle Medium, supplemented with 10% FBS (Biowest, Riverside, United States), 4mM L-Glutamine, 50 U/mL penicillin, and 50 μg/mL streptomycin. In addition, NCI/ADR-RES cells were maintained in media containing 3 μM DOX (Melone Pharmaceutical, Dalian, China). Cells remained free of Mycoplasma and were propagated according to the established protocols.

Hemolytic evaluation

Hemolytic study was performed to evaluate the blood compatibility of **1_3+1_4**/DOX/siRNA nanoballs. The human blood samples were collected from the volunteer in the University of Turku. For hemolysis study, red blood cells were separated by centrifugation at 1200 rpm for 5 min and then washed three times with PBS. After that, red blood cells solution was prepared. Then, 100 μL stock solution was incubated with **1_3+1_4**/DOX/siRNA with different concentrations at 37 °C for 2 h. After incubation, red blood cells were centrifuged at 1200 rpm for 5 min and the supernatants were analyzed at 570 nm were measured by a microplate reader. A phosphate buffer solution was used as a negative control, and the distilled water was used as a positive control. The hemolysis rates were calculated as follows.

$$hemolysis\ rate\ (\%) = \frac{OD_{sample} - OD_{PBS\ buffer}}{OD_{distilled\ water} - OD_{PBS\ buffer}} \times 100\%$$

Where the $OD_{PBS\ buffer}$, OD_{sample} and $OD_{distilled\ water}$ represent the OD values of blank group, treatment group and positive control group, respectively.

Cell uptake by Confocal imaging and Flow cytometry

Confocal laser scanning microscopy (CLSM) and flow cytometry (FC) were used to investigate the internalization of DOX and fluorescence-labeled from **1_3+1_4**/DOX/siRNA (DOX 2 μg/mL, FAM-siRNA: 50 nmol/L). NCI/ADR-RES cell (5×10^4 cells/well) were seeded on the coverslips in 6-well plates and incubated for one night. The free DOX, free FAM-siRNA, **1_3+1_4**/DOX and **1_3+1_4**/DOX/siRNA solutions were added and incubated for 4 h. After that, the cells were fixed for 15 min using 4% paraformaldehyde at room temperature, followed by staining the cell nucleus with a Hoechst 33258 (100 μg/mL). Finally, the coverslips and microscope slides were sealed with a glycerin-water mixture, followed by observation with CLSM.

For the FCM detection, NCI/ADR-RES cells (5×10^4 cells/well) were seeded in 6-well plates and incubated for one night. Then, free DOX, free FAM-siRNA, **1_3+1_4**/DOX and **1_3+1_4**/DOX/siRNA (DOX 2 μg/mL, FAM-siRNA: 50 nmol/L) solutions were added and incubated for 4 h. After that, the cells were rinsed with PBS for three times, trypsinized and collected, followed by suspending in 1 mL deionized water. The samples were finally analyzed using a BD flow cytometer.

Cytotoxicity Characterization

The cytotoxicity of different formations was evaluated by the MTT assay. The cells (8×10^3 cells/well) were seeded in 96-well plates and incubated for one night. Then, free DOX, **1_3+1_4**, free siRNA, **1_3+1_4**/DOX and **1_3+1_4**/DOX/siRNA were added and incubated for 24 h or 48 h, respectively. The medium was set as the control group. After that, 10μL MTT solution (5 mg/mL) was added and incubated for 3 h. Then, the culture medium was replaced by 100 μL DMSO, and the optical

density (OD) values at 570 nm were measured by a microplate reader. Cell viability (CV) was calculated as follows.

$$CV(\%) = \frac{OD_{sample} - OD_{blank}}{OD_{control} - OD_{blank}} \times 100\%$$

Where the OD_{blank}, OD_{sample} and $OD_{control}$ represent the OD values of blank group, treatment group and control group, respectively.

P-gp Silencing Efficiency

The P-gp silencing effect of **1_3+1_4**/DOX/siRNA was investigated by the western blotting method. Briefly, the NCI/ADR-RES cells (10^5 cells/well) were seeded in a 6-well plate, and different formations were added to allow transfection. Then NCI/ADR-RES cells were washed using precooled PBS and solubilized with a lysis buffer. The protein was obtained and the concentration was determined by BCA protein assay kit. The protein was separated using sodium dodecyl sulfate polyacrylamide gel electrophoresis (SDS-PGE) and transferred to a polyvinylidene difluoride (PVDF) membrane. The membrane was blocked, incubated with primary antibody and secondary antibody, and finally visualized using enhanced chemiluminescence (ECL).

Apoptotic Analysis

NCI/ADR-RES cell (10^5 cells/well) were seeded on the coverslips in 6-well plates and incubated for one night. The free DOX, free siRNA, **1_3+1_4**, free siRNA, **1_3+1_4**/DOX and **1_3+1_4**/DOX/siRNA solutions were added and further incubated for 24 h. After that, the cells were trypsinized, collected and washed with PBS, and Annexin binding buffer for three times. Then, 5μL Annexin V-FITC was added into each cell suspension (100 μL) and stained for 15 min at room temperature. Then 10 μL PI was added into each cell suspension. After that, the cell suspension was added into 1 mL PBS solution, and evaluated by FCM.

Statistical analysis

All experimental data were performed in triplicate, and the data were expressed as mean ± standard deviation, where applicable. Data were statistically processed expressed using one way analysis of variance (ANOVA) to assess significant differences among various groups followed by student t-test using Origin Pro 8.6 software.

2. Synthesis and Characterization of building block 1

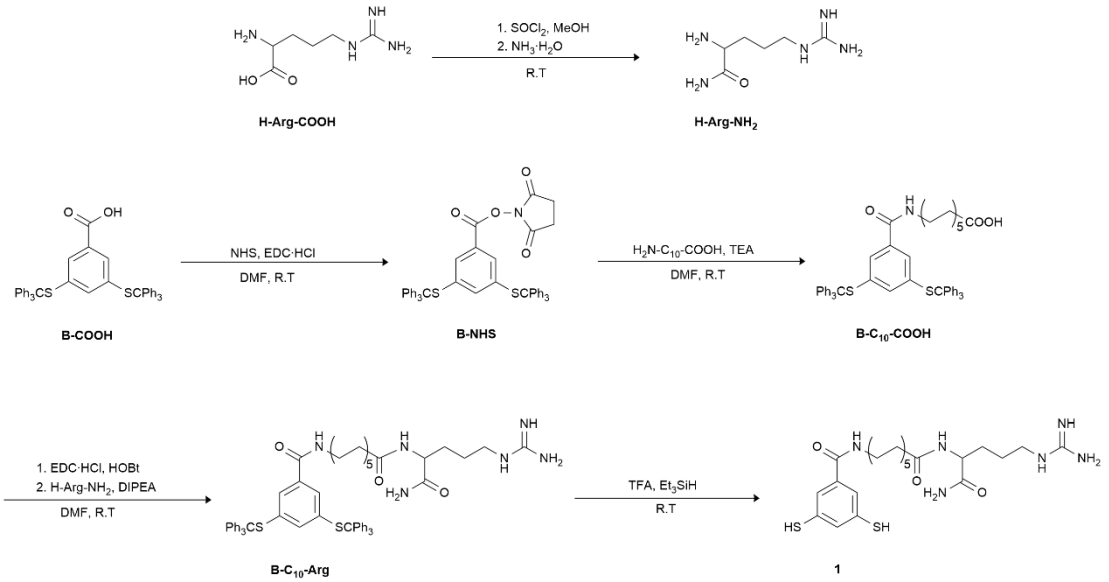

Scheme S1. The synthesis route of **1**

2.1 H-Arg-NH_2

The synthesis of H-Arg-NH_2 was according to the previous report. [S2] Arginine (2.613 g, 15 mmol) was suspended in methanol (20 mL) and cooled in an ice bath. Then $SOCl_2$ (1.5 mL, 20 mmol) was added in the solution drop by drop. The reaction was stirred at room temperature and monitored by TLC. After the reaction was finished, the solvent was removed under reduced pressure. The obtained H-Arg-OMe was yellowish paste and did not need to further purification. ^{1}H NMR (500 MHz, D_2O, 298K) δ (ppm): 4.22 (t, J=6.42Hz, 1H), 3.88 (s, 3H), 3.28 (t, J=6.81 Hz, 2H), 2.10-1.97 (m, 2H), 1.83-1.67 (m, 2H).

Saturated ammonium hydroxide aqueous solution (10 mL, 65 mmol) was added, the resulting solution was stirred at room temperature until the reaction was complete. The solution was concentrated and the residue was purified by recrystallization from ice ethyl ether to get H-Arg-NH_2. The final product was white powder (2.51 g) with ~96% yield in total. ^{1}H NMR (500 MHz, D_2O, 298K) δ (ppm): 3.98 (t, J=6.50Hz, 1H), 3.28 (t, J=6.85, 2H), 1.96-1.90 (m, 2H), 1.75-1.69 (m, 2H).

2.2 B-NHS

2,5-bis(trithyltio)benzoic acid (1.610 g, 2.4 mmol) and NHS (1.104 g, 9.6 mmol) were dissolved in anhydrous DMF (80 mL) in an ice bath. Then EDC·HCl (1.84 g, 9.6 mol) was added in the solution and the mixture was stirred at room temperature overnight. The reaction was monitored by TLC. When the rection was finished, the solution was poured into 200 mL deionized water, and adjusted pH to 3 by 1M HCl solution. The white solid (1.57 g) was obtained by filtrated with ~86% yield. ^{1}H NMR (500 MHz, DMSO, 298K) δ (ppm): 7.26-7.20 (m, 30H), 7.09 (s, 1H), 7.06 (d, J=1.50 Hz, 2H), 2.83 (s, 4H).

2.3 B-C_{10}-COOH

B-NHS (650 mg, 0.84 mmol) and 11-aminoundecanoic acid (844 mg, 4.2 mmol) were dissolved in anhydrous DMF (20 mL), then TEA (588 μL, 4.2 mmol) was added in the solution. The mixture was continuous stirred overnight at room temperature and monitored by TLC. After the reaction was finished, DCM (50 mL) was added and the solution was washed with 1M HCl (30 mL), saturated $NaHCO_3$ (30 mL) and water (30 mL). The organic phase was dried by $MgSO_4$ and concentrated under pressure. The residue was purified was dissolved in DCM and purified by flash column chromatography to obtain the product as a white solid (560 g) with ~78% yield. ^{1}H NMR (500 MHz, $CDCl_3$, 298K) δ (ppm): 7.32-7.29 (m, 12H), 7.19-7.17 (m, 18H), 7.09 (t, J=1.48Hz, 1H), 6.80 (d, J=1.55 Hz, 2H), 5.11 (t, J=5.27 Hz, 1H), 3.20-3.19 (q, J=6.65 Hz, 2H), 2.35 (t, J=7.43 Hz, 2H), 1.64 (p, J=7.25 Hz, 2H), 1.45 (p, J=7.25Hz, 2H), 1.37-1.29 (m, 12 H). ^{13}C NMR (125 MHz, $CDCl_3$, 298K) δ (ppm): 177.36, 166.06, 144.30, 142.23, 135.02, 134.35, 132.26, 130.08, 127.92, 126.92, 71.38, 39.95, 33.78, 29.65, 29.47, 29.38, 29.27, 29.20, 29.08, 26.00, 24.83. ESI-QTOF $[M+Na]^+$ found: 876.3585 (expected:876.3521).

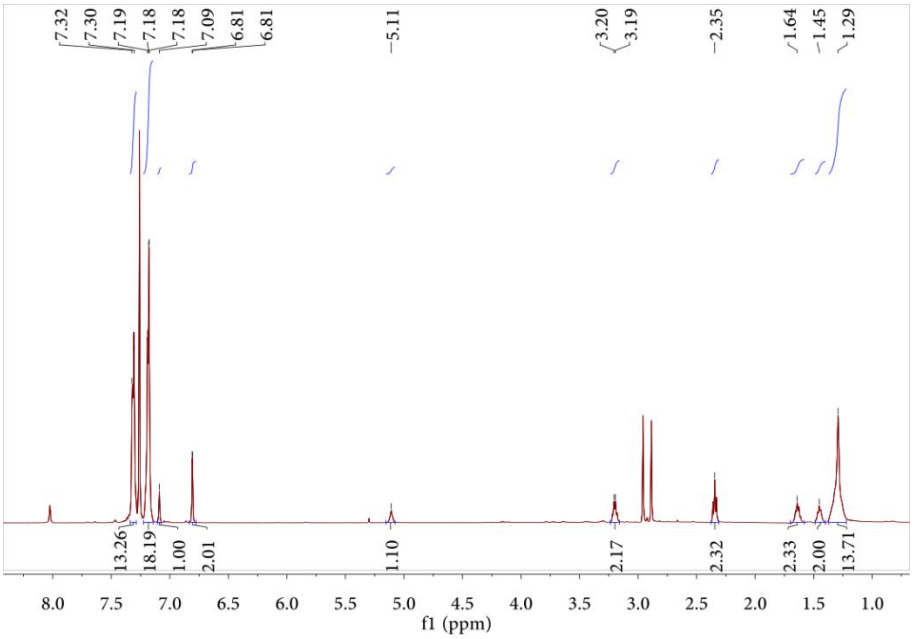

Figure S1. ^{1}H NMR of B-C_{10}-COOH (500 MHz, $CDCl_3$).

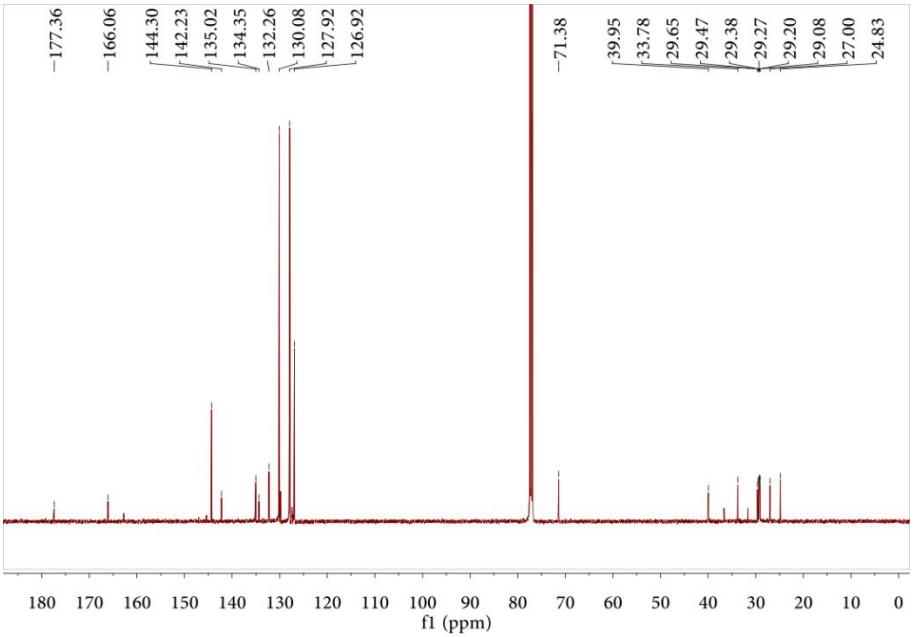

Figure S2. ^{13}C NMR of B-C_{10}-COOH (125 MHz, $CDCl_3$).

2.4 B-C_{10}-Arg

B-C_{10}-COOH (717 mg, 0.84 mmol) and H-Arg-NH_2 (295 mg, 1.7mmol) were dissolved in anhydrous DMF (15 mL) in an ice bath. Then HOBt (229.5 mg, 1.7 mmol), EDC·HCl (326.4mg, 1.7 mmol) and DIPEA (457 μL, 3.4 mmol) were added in the solution. The mixture was stirred overnight at room temperature and monitored by TLC. After the reaction was finished, DCM (50 mL) was added and the solution was washed with 1M HCl (30 mL), saturated $NaHCO_3$ (30 mL) and water (30 mL). The organic phase was dried by $MgSO_4$ and concentrated under pressure. The residue was purified was dissolved in DCM and purified by flash column chromatography to obtain the product as a white solid (0.49 g) with ~58% yield. ^1H NMR (500 MHz, $CDCl_3$, 298K) δ (ppm): 7.32-7.28 (m, 12H), 7.20-7.13 (m, 19H), 6.78 (s, 2H), 5.39 (br s, 1H), 3.28 (br s, 2H), 3.12 (br s, 2H), 2.24 (br s, 2H), 1.92-1.70 (m, 4H), 1.51 (br s, 2H), 1.39 (br s, 2H), 1.25-1.19 (m, 12H). ^{13}C NMR (125 MHz, $CDCl_3$, 298K) δ (ppm):147.00, 145.40, 144.24, 135.06, 132.46, 130.04, 129.82, 128.08, 127.92, 127.86, 127.41, 126.93, 71.43, 53.84, 40.19, 37.29, 35.73, 29.74, 29.55, 29.47, 27.11, 18.83. ESI-QTOF $[M+H]^+$ found: 1009.4840 (expected:1009.4873).

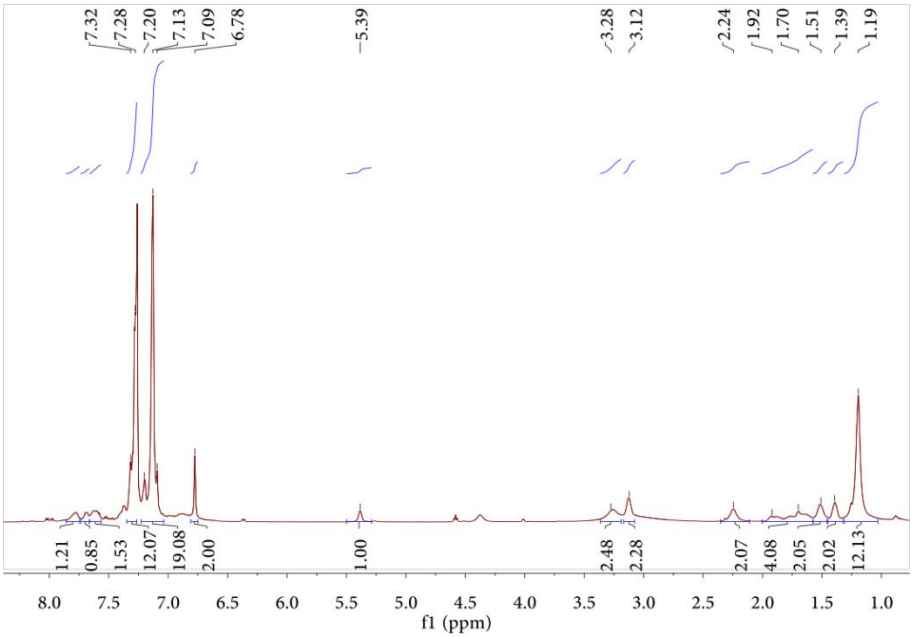

Figure S3. ^{1}H NMR of B-C_{10}-Arg (500 MHz, $CDCl_3$).

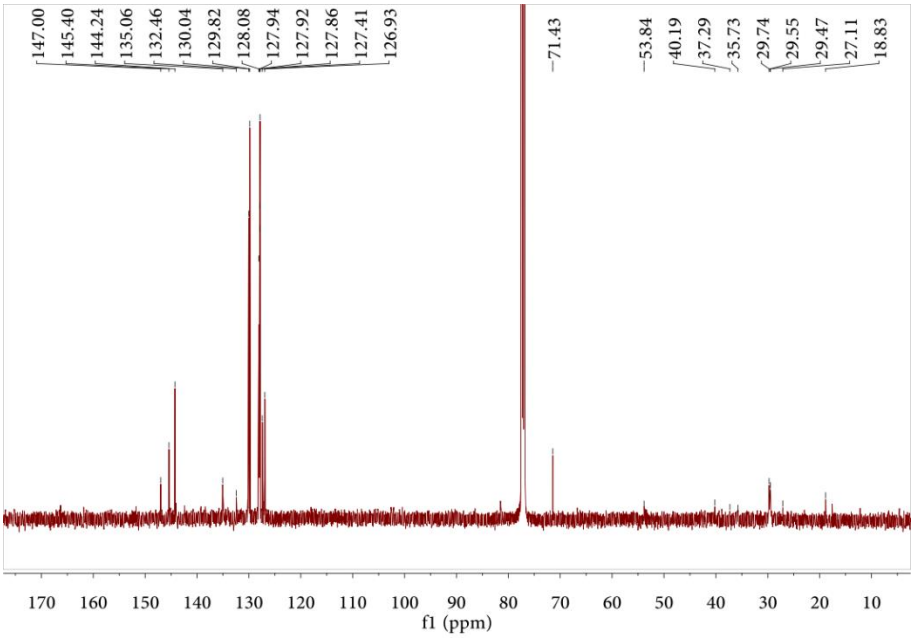

Figure S4. ^{13}C NMR of B-C_{10}-Arg (125 MHz, $CDCl_3$).

2.5 Building block 1

3 mL TFA was degassed through three freeze-pump-thaw cycles and added into a 25 mL round bottom flask containing B-C_{10}-Arg (100 mg, 99.1 mmol) under nitrogen. The organic solution was sonicated for 5 minutes and stirred at room temperature for 15 minutes. Then Et_3SiH (200 µL, 1.25 mmol) was added and the solution was stirred for 15 minutes. TFA was removed under pressure and the suspension was dissolved in 20 mL of a degassed mixture of MeOH-H_2O (9:1). The solution

was washed with petroleum ether for three times. Methanol was removed by rotary evaporator and the suspension was freeze-dried for 48 h to furnish the corresponding building block (30.9 mg) with ~59% yield. ^{1}H NMR (500 MHz, CD_3OD, 298K) δ (ppm): 7.38 (s, 2H), 7.31 (s, 1H), 4.33 (q, J=4.57Hz, 1H), 3.16-3.15 (q, J=6.96 Hz, 2H), 2.21 (t, J=4.97 Hz, 2H), 1.81 (m, J=3.63 Hz, 1H), 1.71-1.63 (m, 6H), 1.32-1.28 (m, 12 H). ^{13}C NMR (125 MHz, CD_3OD, 298K) δ (ppm): 176.55, 176.41, 168.94, 158.64, 137.44, 135.29, 131.76, 124.99, 53.58, 41.97, 41.04, 36.88, 30.55, 30.50, 30.39, 30.34, 30.31, 28.01, 26.86, 26.36. ESI-QTOF $[M+H]^+$ found: 525.2641 (expected: 525.2682).

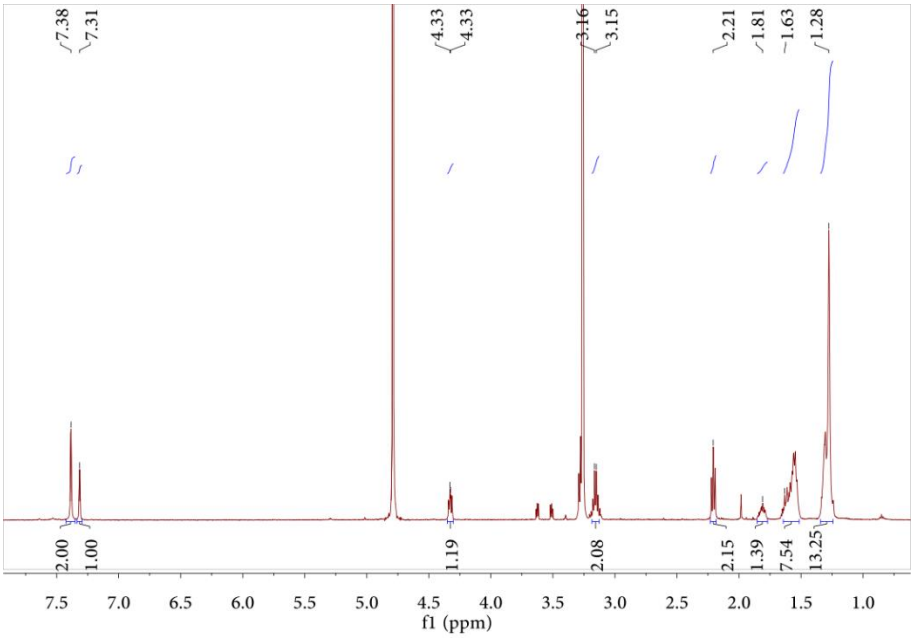

Figure S5. ^{1}H NMR of **1** (500 MHz, CD_3OD).

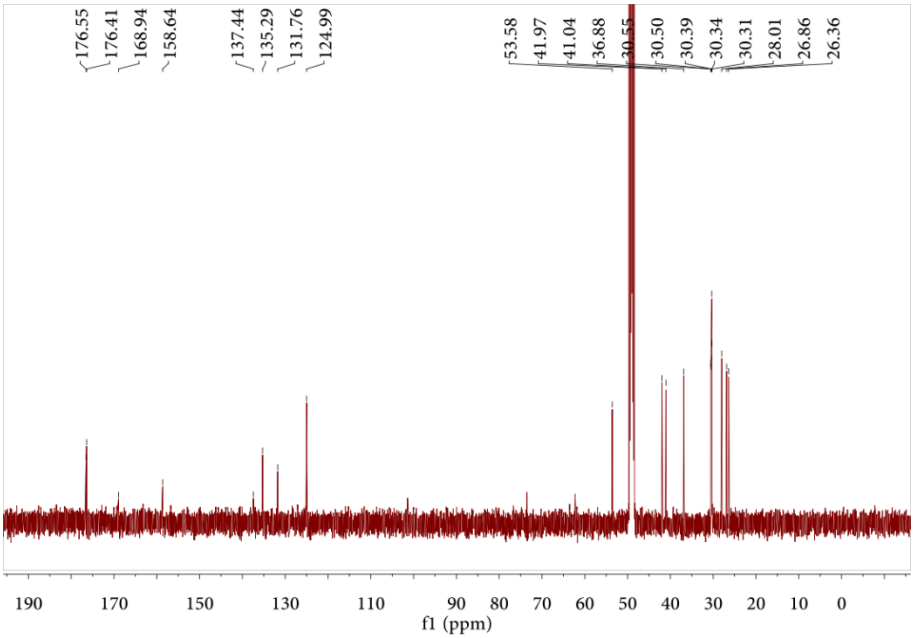

Figure S6. ^{13}C NMR of **1** (125 MHz, CD_3OD).

3. HPLC, mass analysis and ^{1}H NMR of 1_3+1_4.

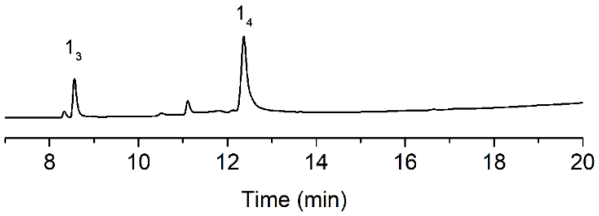

Figure S7. HPLC of a DCL made from building block **1**.

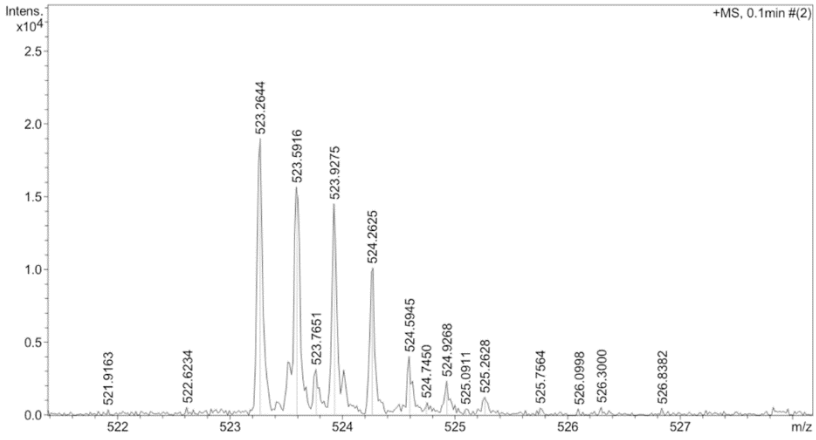

Figure S8. Mass spectrum of **Trimer 1_3** from the HPLC-MS analysis of a DCL made from building block **1**. m/z calculated for $[M+3H]^{3+}$, 523.2525, found 523.2644.

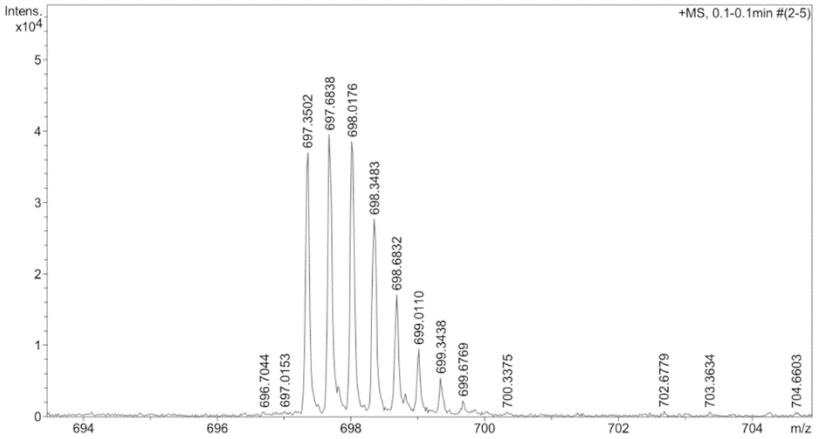

Figure S9. Mass spectrum of **Tetramer 1_4** from the HPLC-MS analysis of a DCL made from building block **1**. m/z calculated for $[M+3H]^{3+}$, 697.6686, found 697.6838.

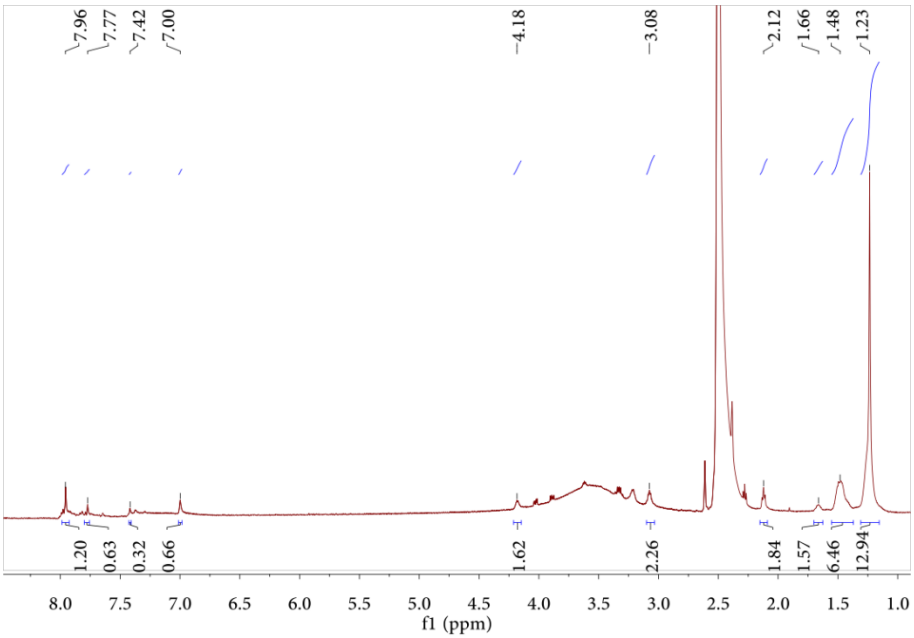

Figure S10. ^{1}H NMR of **1**$_3$+**1**$_4$ (500 MHz, DMSO).

4. HPLC of reduced 1

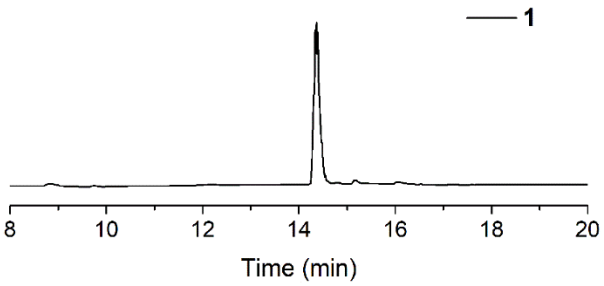

Figure S11. HPLC of **1** which is reduced from polymer by DTT.

5. TEM analysis of 1_3+1_4 and 1_3+1_4/DOX and 1_3+1_4/DOX/siRNA

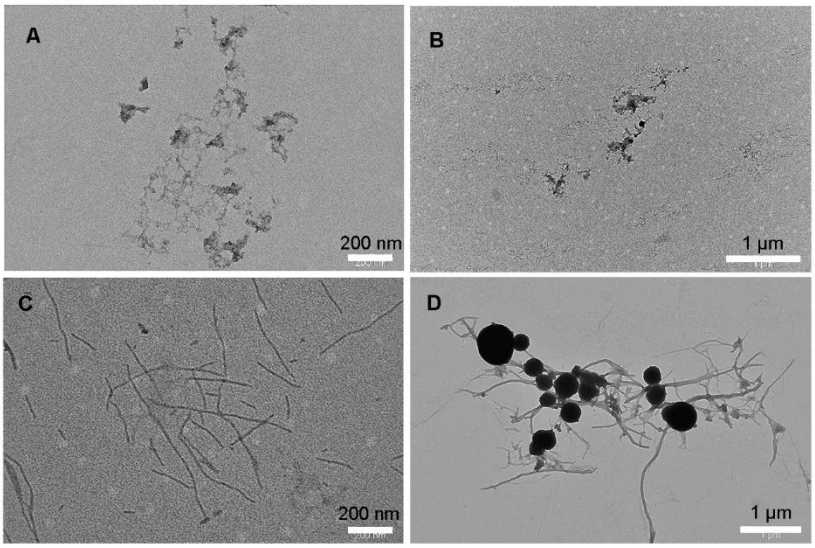

Figure S12. TEM micrography of nanostructures from (A-B) **1_3+1_4** and (C) **1_3+1_4**/DOX nanofibers and (D) **1_3+1_4**/DOX/siRNA nanoballs. Bar scale in A and C, 200 nm; B and D, 1 μm.

6. Molecular modeling of 1_3 and 1_4 by Chem 3D

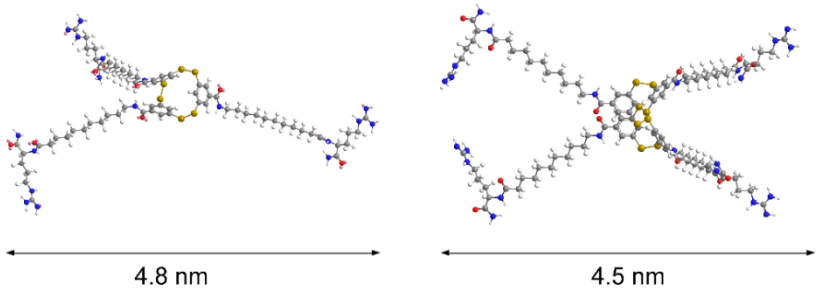

Figure S13. Molecular model of **1_3** and **1_4** by Chem3D.

7. FT-IR of DOX, 1_3+1_4 and 1_3+1_4/DOX

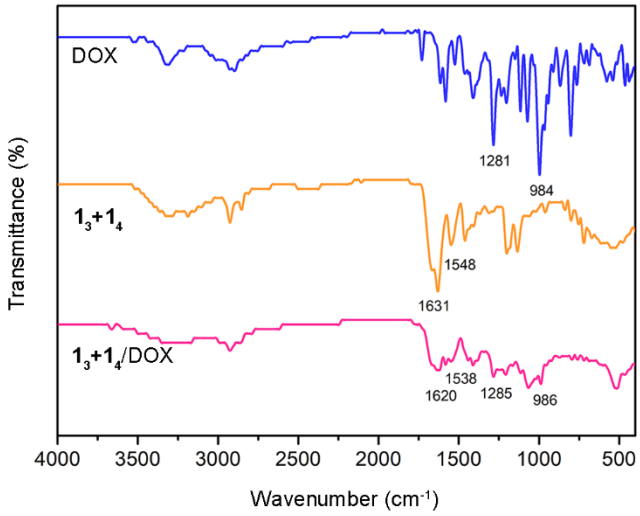

Figure S14. FT-IR spectrum of DOX, **1_3+1_4** and **1_3+1_4**/DOX.

8. Agarose gel electrophoresis assay of 1_3+1_4/DOX/siRNA system

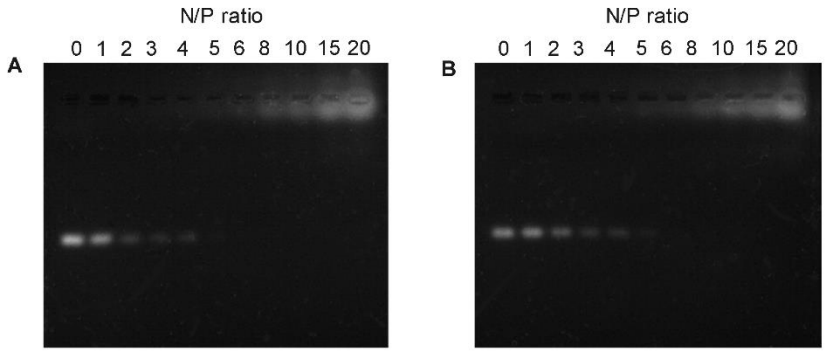

Figure S15. Agarose gel electrophoresis assay of **1_3+1_4**/DOX/siRNA with different N/P ratios. (A) Binding capability assay of **1_3+1_4**/DOX/siRNA with different N/P ratios; (B) Heparin stability assay of **1_3+1_4**/DOX/siRNA with different N/P ratios.

9. PXRD of 1_3+1_4/DOX/siRNA

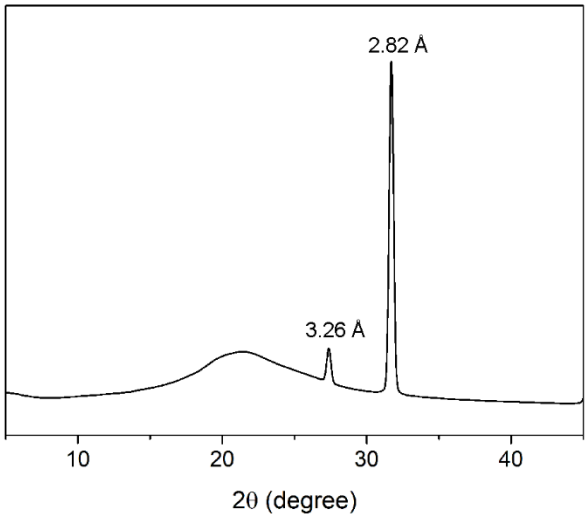

Figure S16. PXRD of **1_3+1_4**/DOX/siRNA nanoballs.

10. Particle size and zeta potential of 1_3+1_4 and 1_3+1_4/DOX and 1_3+1_4/DOX/siRNA

Table S1. Characterization of different formations by DLS.

Sample	Z-Average (nm)	Polydispersity Index	Zeta Potential (mV)
1_3+1_4	1357.0±87.7	0.829±0.047[a]	19.03±0.68
1_3+1_4/DOX	683.0±92.0[b]	0.587±0.042	17.70±0.61
1_3+1_4/DOX/siRNA	298.1±37.1	0.470±0.040	16.93±0.06

[a]The polydispersity index (PDI) of **1_3+1_4** is over 0.8, which means that the sample has a very wide size distribution.

[b]The large Z-average size of **1_3+1_4**/DOX is due to the long length of nanofibers.

11. Redox- and pH-induced release of DOX and siRNA from 1_3+1_4/DOX/siRNA system

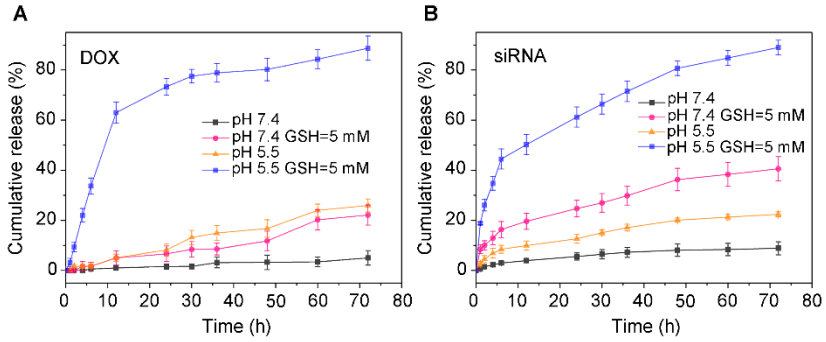

Figure S17. *In vitro* redox- and pH-induced release of DOX and siRNA from **1_3+1_4**/DOX/siRNA system. (A) DOX release from **1_3+1_4**/DOX/siRNA at different conditions; (B) siRNA release from **1_3+1_4**/DOX/siRNA at different conditions. All of the measurements were performed in triplicate; error bars represent SDs about the mean.

12. Hemolytic study of 1_3+1_4/DOX/siRNA system

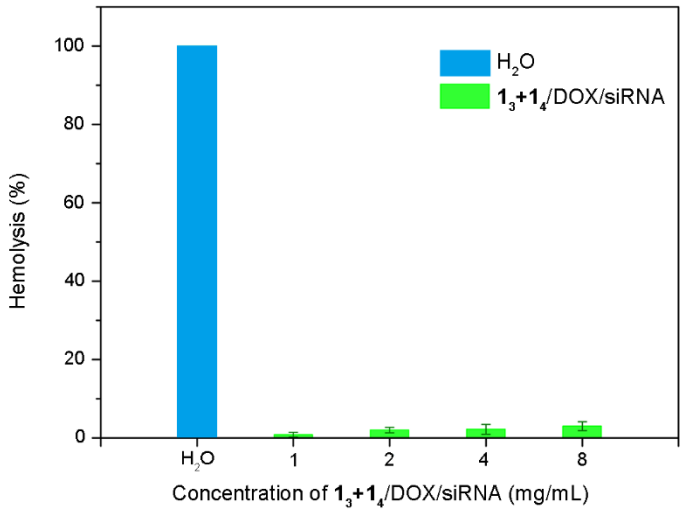

Figure S18. Blood compatibility of **1_3+1_4**/DOX/siRNA nanoballs. All of the measurements were performed in triplicate; error bars represent SDs about the mean.

13. Cytotoxicity assay of 1_3+1_4 in NCI/ADR-RES cells

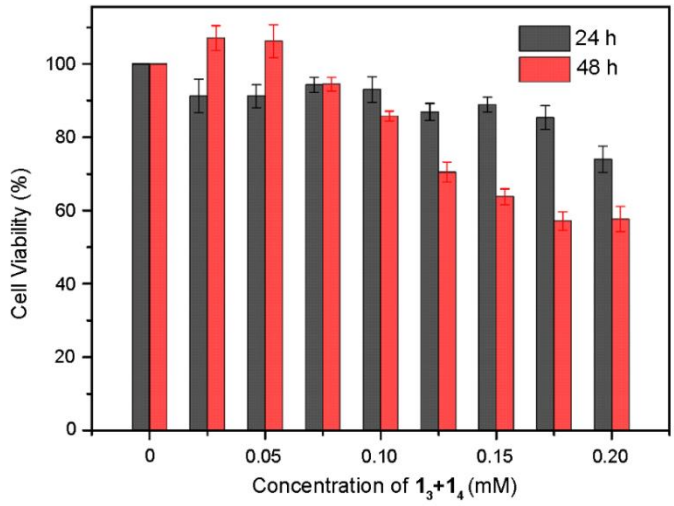

Figure S19. Cell viability assay of NCI/ADR-RES cells incubated with **1_3+1_4** (**1_3+1_4** concentration ranging from 0.025 mM to 0.2 mM). All of the measurements were performed at least in triplicate; error bars represent SDs about the mean.

14. Cytotoxicity assay of 1_3+1_4 in HEK293 cells

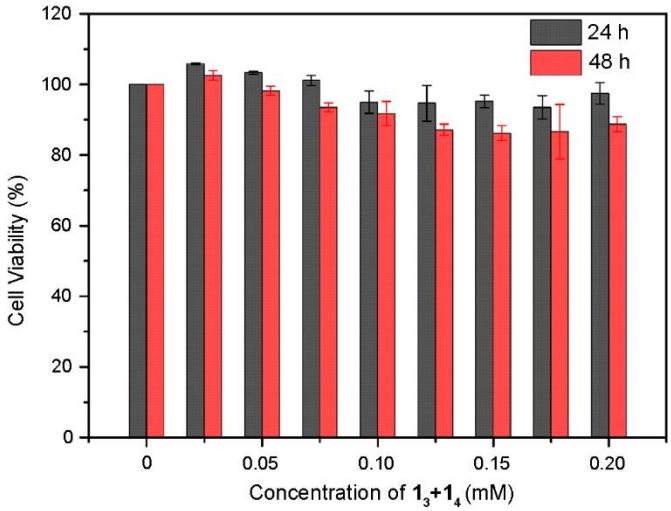

Figure S20. Cell viability assay of HEK293 cells incubated with **1_3+1_4** (**1_3+1_4** concentration ranging from 0.025 mM to 0.2 mM). All of the measurements were performed at least in triplicate; error bars represent SDs about the mean.

15. In vitro anti-cancer effect of 1_3+1_4/DOX/siRNA system in MCF-7S cells

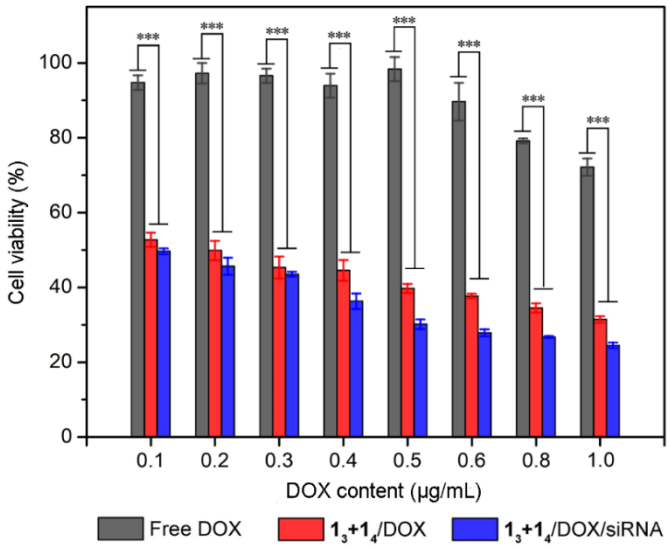

Figure S21. *In vitro* anticancer efficacy. MCF-7S Cells were incubated with DOX, **1_3+1_4**/DOX and **1_3+1_4**/DOX/siRNA for 24 h. All of the measurements were performed at least in triplicate; error bars represent SDs about the mean. *P<0.05, **P<0.01, and ***P<0.001.

16. Apoptosis-induced Anticancer activity of 1_3+1_4/DOX/siRNA in NCI/RES-ADR cells

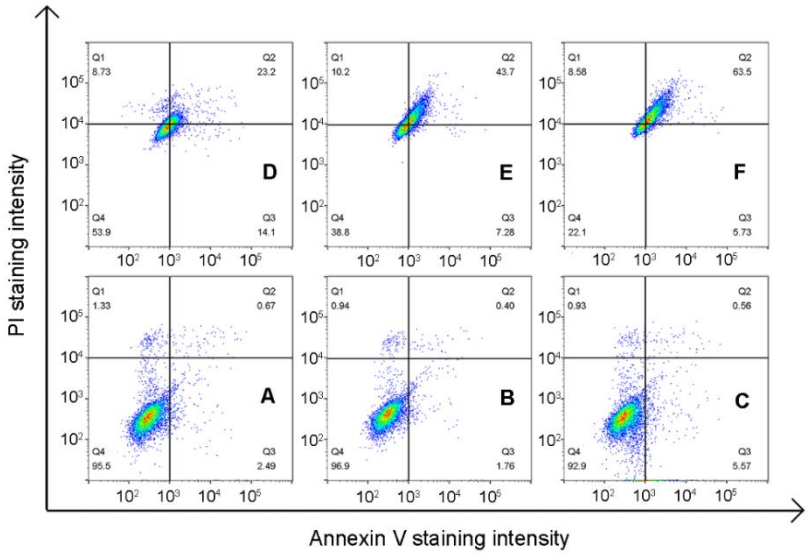

Figure S22. Apoptotic analysis of NCI/ADR-RES cells by FC. NCI/ADR-RES cells were treated with (A) control, (B) free siRNA, (C) **1_3+1_4**, (D) free DOX, (E) **1_3+1_4**/DOX and (F) **1_3+1_4**/DOX/siRNA for 24 h, and then incubated with Annexin V-FITC and PI.

17. Reference

[S1] Mansfeld, F.M., Feng, G., and Otto, S. (2009). Photo-induced molecular-recognition-mediated adhesion of giant vesicles. Org. Biomol. Chem. *7*, 4289-4295.

[S2] Zhang, T., Song, W., Zhao, J., and Liu, J. (2017). Full Solution-Phase Synthesis of Acetyl Hexapeptide-3 by Fragments Coupling Strategy. Ind. Eng. Chem. Res. *56*, 11697-11704.